NASA TECHNICAL REPORT

NASA TR R-445

NASA TR R-445

FOUR METHODS OF ATTITUDE DETERMINATION FOR SPIN-STABILIZED SPACECRAFT WITH APPLICATIONS AND COMPARATIVE RESULTS

Gene A. Smith

Goddard Space Flight Center
Greenbelt, Md. 20771

NATIONAL AERONAUTICS AND SPACE ADMINISTRATION • WASHINGTON, D. C. • AUGUST 1975

1. Report No.	2. Government Accession No.	3. Recipient's Catalog No.
NASA TR R-445		

4. Title and Subtitle	5. Report Date
Four Methods of Attitude Determination for Spin-stabilized Spacecraft with Applications and Comparative Results	August 1975
	6. Performing Organization Code: 560
7. Author(s): Gene A. Smith	8. Performing Organization Report No.: G-7522
9. Performing Organization Name and Address: Goddard Space Flight Center, Greenbelt, Maryland 20771	10. Work Unit No.: 311-07-14-01
	11. Contract or Grant No.
	13. Type of Report and Period Covered: Technical Report
12. Sponsoring Agency Name and Address: National Aeronautics and Space Administration, Washington, D. C. 20546	14. Sponsoring Agency Code

15. Supplementary Notes

16. Abstract

The attitude of a spacecraft is determined by specifying three independent parameters which relate the spacecraft axes to an inertial coordinate system. One convenient set of orientation parameters for spin-stabilized satellites consists of the spin rate, inertial space coordinates of the spin axis, $\vec{S}$, and another spacecraft vector, $\vec{V}$; these parameters change with time and must be known at a particular time. On spacecraft for which the spin rate and $\vec{V}$ are measured directly by the onboard sensors, the attitude problem reduces to determining the spin axis, $\vec{S}$.

One class of sensors measures angles between $\vec{S}$ and other vectors directed to objects or fields external to the spacecraft. Two of these sensor angles and the known inertial coordinates of the associated objects or fields are sufficient for determining the components of $\vec{S}$. For the spin-stabilized spacecraft considered here, $\vec{S}$ is constant over at least an orbit, but separate solutions based on sensor angle measurements are different due to propagation of errors. Some of the sensor-angle solution methods currently in use minimize the propagated errors by making use of least-squares techniques over many sensor-angle measurements and by solving explicitly (in closed form) for the spin axis coordinates. Comparison of these methods with star observation solutions is necessary to determine if satisfactory accuracy is obtained by each method.

17. Key Words (Selected by Author(s))	18. Distribution Statement
Mathematics; Space sciences; Space vehicles; Spin-stabilized spacecraft; Attitude determination	Unclassified – Unlimited CAT. 18

19. Security Classif. (of this report)	20. Security Classif. (of this page)	21. No. of Pages	22. Price*
Unclassified	Unclassified	71	$4.25

*For sale by the National Technical Information Service, Springfield, Virginia 22161

This document makes use of international metric units according to the Systeme International d'Unites (SI). In certain cases, utility requires the retention of other systems of units in addition to the SI units. The conventional units stated in parentheses following the computer SI equivalents are the basis of the measurements and calculations reported.

CONTENTS

FOUR METHODS OF ATTITUDE DETERMINATION FOR SPIN–STABILIZED SPACECRAFT WITH APPLICATIONS AND COMPARATIVE RESULTS

Gene A. Smith
Goddard Space Flight Center

FORMULATION OF PROBLEM

Spacecraft Attitude

The attitude of a spacecraft is defined by the specification of three rotation angles relating the spacecraft axes to a known coordinate system. These rotation angles are Eulerian, and as such are not unique but are chosen for convenience or naturalness. (For further discussion of Eulerian angles and their nonuniqueness, see Appendix A and references 1 and 2.)

A number of well defined coordinate systems are available for attitude design considerations. The most convenient of these systems are those with inertial space coordinates, which have the advantage of being constant with time and are related to the celestial sphere. The two most common systems are the equatorial inertial (Z = north pole, X = first point of Aries, and Y = perpendicular to XZ plane to form a right-handed system) and the ecliptic inertial (Z = ecliptic north pole, X = first point of Aries, and Y as above).

The spacecraft axes are chosen with regard to the design, function, moments of inertia, and planned orientation of the spacecraft, and are fixed with respect to the satellite body. As examples, a pointing spacecraft has the pointing direction defined as one axis (usually the X-axis), and the spinning spacecraft, discussed in this paper, has its spin axis defined as the Z-axis.

Thus, with selection of the body-fixed spacecraft axes, the appropriate external coordinate system, and a set of rotation angles, the spacecraft attitude can be described unambiguously.

Spin-stabilization

If a spacecraft is spun about its largest principal moment of inertia, this spin axis will point in the same direction in inertial space unless acted upon by torque-producing forces. For most earth-orbiting spacecraft, gravitational forces are nearly constant, with the slight deviations adding to other variant forces to create spacecraft torques. These are relatively small perturbations which give rise to slowly varying spin-axis orientations. By slowly varying is meant a time much longer than the spin period, such that the spacecraft orientation does not become unstable. This condition is called spin stabilization.

The design of the satellite and the proposed orbit are critical considerations in preventing torques from becoming disruptive to the spin stability. Thus, antennas and booms are kept

light and short, to keep gravitational torques small; magnetic moments are balanced; and the orbit is high enough to make air drag negligible. In addition, some error in alignment of the maximum moment of inertia with the symmetric body axis, about which the spacecraft is spun, is common and produces a coning of the spin axis about the net angular momentum vector. (See reference 2, pp. 113-125.) In this report it is assumed that external torques are negligible, that initial spacecraft oscillations have been damped, and that misalignment effects are less than other error sources.

Spin-stabilized Spacecraft Attitude

In the case of a spacecraft spinning about its largest principal moment of inertia, the spin axis is defined as the z-axis (figure 1). To transform the orthogonal spacecraft coordinates, xyz, into the orthogonal equatorial inertial coordinates, XYZ, choose the Eulerian rotation angles θ, $\overline{\delta}$, and $-\alpha$ where they are defined as follows: First, rotate the x-axis counterclockwise (ccw) by the arc θ around the z-axis, to bring the x-axis into the Zz plane and the y-axis into the XY plane and perpendicular to the Zz plane. Second, rotate ccw around the new y-axis by $\overline{\delta}$ to make the z-axis coincident with the Z. Third, rotate clockwise (cw) around the final z (=Z) axis by $-\alpha$ to complete the transformation.

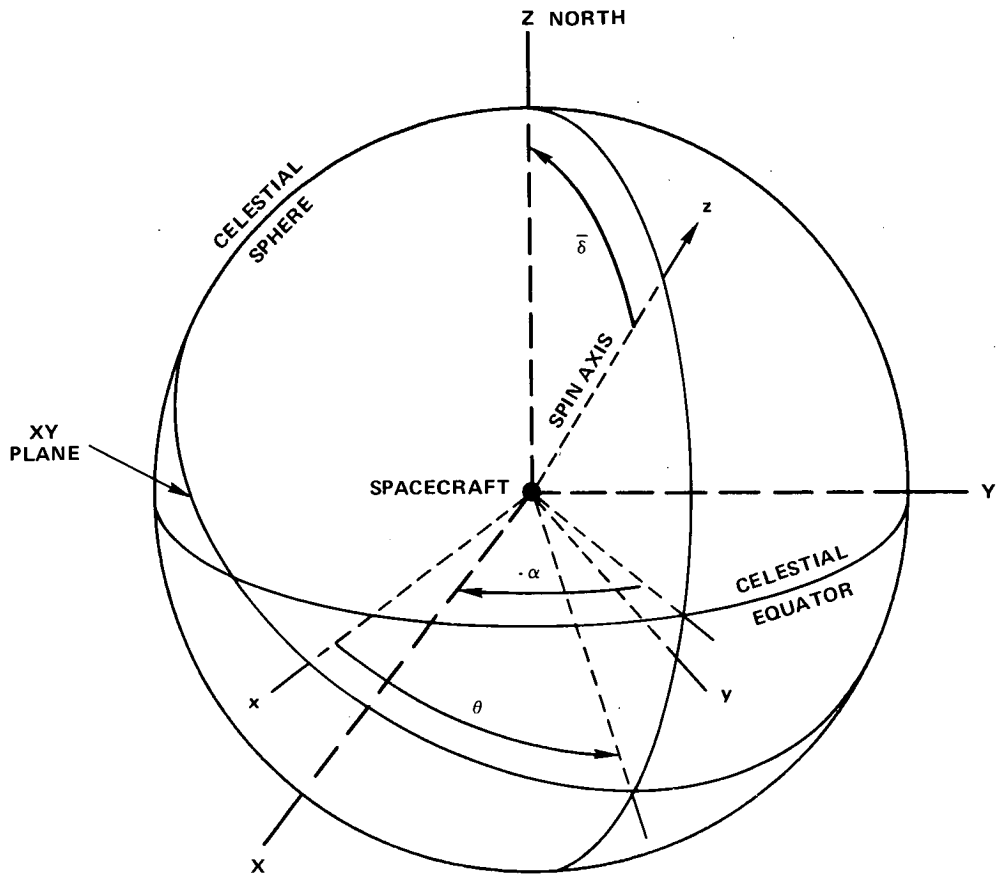

Figure 1. Spacecraft Axes, x, y, z, Referenced to Inertial Coordinates, X, Y, Z

In matrix notation, the transformation is

$$\underset{R(\alpha)}{\begin{bmatrix} \cos\alpha & -\sin\alpha & 0 \\ \sin\alpha & \cos\alpha & 0 \\ 0 & 0 & 1 \end{bmatrix}} \underset{R(\bar{\delta})}{\begin{bmatrix} \cos\bar{\delta} & 0 & -\sin\bar{\delta} \\ 0 & 1 & 0 \\ \sin\bar{\delta} & 0 & \cos\bar{\delta} \end{bmatrix}} \underset{R(\theta)}{\begin{bmatrix} \cos\theta & \sin\theta & 0 \\ -\sin\theta & \cos\theta & 0 \\ 0 & 0 & 1 \end{bmatrix}} \begin{bmatrix} x \\ y \\ z \end{bmatrix} = \begin{bmatrix} X \\ Y \\ Z \end{bmatrix}$$

with $R(\alpha)\, R(\bar{\delta})\, R(\theta) = R(t)$

where

$$R(t) = \begin{bmatrix} \cos\alpha\ \cos\bar{\delta}\ \cos\theta + \sin\alpha\ \sin\theta & \cos\alpha\ \cos\bar{\delta}\ \sin\theta - \sin\alpha\ \cos\theta & -\cos\alpha\ \ \sin\bar{\delta} \\ \sin\alpha\ \cos\bar{\delta}\ \cos\theta - \cos\alpha\ \sin\theta & \sin\alpha\ \cos\bar{\delta}\ \sin\theta + \cos\alpha\ \cos\theta & -\sin\alpha\ \ \sin\bar{\delta} \\ \sin\bar{\delta}\ \cos\theta & \sin\bar{\delta}\ \sin\theta & \cos\bar{\delta} \end{bmatrix}.$$

For the transformation of the z-axis only (that is, X, Y, and Z components of a vector parallel to the z-axis and x = y = 0),

$$R(t) \begin{bmatrix} x \\ y \\ z \end{bmatrix} = R(t) \begin{bmatrix} 0 \\ 0 \\ z \end{bmatrix} = \begin{bmatrix} X \\ Y \\ Z \end{bmatrix}$$

which yields the three equations

$$\begin{aligned} -\cos\alpha\ \sin\bar{\delta}\ z &= X \\ -\sin\alpha\ \sin\bar{\delta}\ z &= Y \\ \cos\bar{\delta}\ \ z &= Z \end{aligned}$$

where X, Y, and Z are the components of the vector in inertial coordinates. By convention, the angle α is the right ascension of the spin axis, and the angle $\bar{\delta}$ is the codeclination. The declination is $\delta = (90° - \bar{\delta})$, such that $\bar{\delta} = 90° - \delta$ substituted in the above equations yields

$$-\cos\alpha\ \cos\delta\ z = X;\ -\sin\alpha\ \cos\delta\ z = Y;\ \text{and}\ \sin\delta\ z = Z.$$

The solution of δ and α are then given by

$$\frac{-\sin\alpha}{-\cos\alpha} = \tan\alpha = \frac{Y}{X}$$

or

$$\alpha = \tan^{-1}\frac{Y}{X}$$

and

$$\sin \delta \; z = Z$$

or

$$\delta = \sin^{-1} \frac{Z}{z}$$

where

$$z^2 = X^2 + Y^2 + Z^2 .$$

Thus, the spin axis direction can be determined either by finding components in the desired reference coordinate system or by solving for the spin axis right ascension and declination.

The remaining constituent of spin-stabilized spacecraft attitude is the rotation around z, represented above by θ, which brings the x-axis into the Zz plane.

Sensor Angles

One type of spacecraft sensor measures angles between the spin axis and external physical objects or fields, such as the sun or the magnetic field. These sensor angles are related to each other in such a way as to make it possible to solve for the spin axis.

If three different sensors supply the angles, unambiguous solutions are possible. However, the use of only two different sensors is preferred, though this produces two-solution ambiguities, since one solution can be eliminated by physical arguments, and the savings to the spacecraft in space and cost are significant.

Cone Intersection Interpretation

The reason that two different sensor angles characterize the spin-axis attitude with a two-solution ambiguity, while three sensor angles remove the ambiguity and a single sensor gives no useful solutions, is shown by reference to a geometrical argument. (See figure 2.)

If the coordinates of a vector $\vec{P}$ are known in inertial space, and a sensor angle ξ is measured between $\vec{P}$ and the spin axis $\vec{S}$, then the direction of $\vec{S}$ is known to project onto the celestial sphere at some point on a circle of angular radius ξ circumscribing $\vec{P}$.

If two sensor angles, ξ and η, are measured between $\vec{P}$ and $\vec{S}$ and between $\vec{Q}$ and $\vec{S}$, respectively, where $\vec{P}$ and $\vec{Q}$ are known, then the possible orientations of $\vec{S}$ are at the points of intersection of the two cones tracing out the circles of radii ξ and η on the celestial sphere. Except for the degenerate case when $\vec{P}$ and $\vec{Q}$ become colinear (within the resolution limits of the sensors) and the sensor angles, ξ and η, become equal, at least one intersection of the two cones is produced. The one-intersection occurrence is infrequently measured, so that a two-solution ambiguity is the general case to be considered in cone-intersection attitude determination.

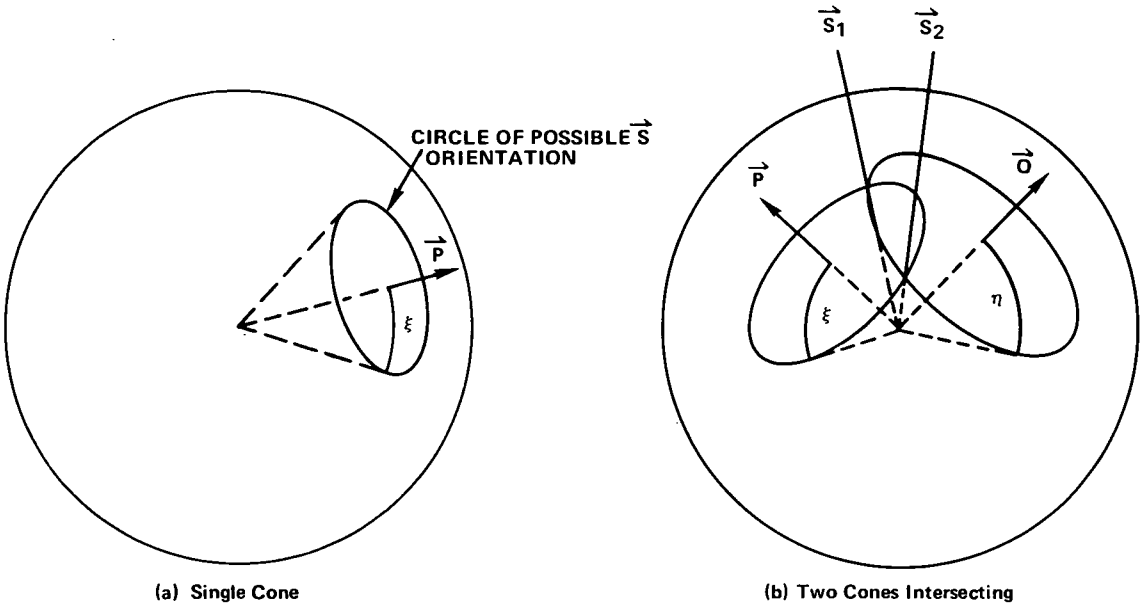

(a) Single Cone

(b) Two Cones Intersecting

Figure 2. Sensor Angle Cones

One solution can normally be eliminated by considering the past history of the spin axis. That is, if the inertial spin axis is a consequence of post-launch procedures, then subsequent correct solutions are close to the previous ones, and the unacceptable cone-intersection solutions vary rapidly with time. Alternatively, if the time between observations of $\vec{P}$ and $\vec{Q}$ is measured, the ambiguity is resolved since the angular separation of the sensors is known.

After reorientation of the spin axis by ground controlled spacecraft torques, the correct solution is again uncertain. Predictions of the effect of the torque should indicate one solution as preferable. However, difficulties arise as the intersections draw together, merge, and then part. Uncertainty as to the best solution or series of solutions leads to many different ways of analyzing the sensor angle data and will not be pursued at this time.

A requirement on the sensor angles due to the motion of the spin axis orientation is that they be measured close to the same time—of the order of a spin period. This ensures that the actual spin axis will not have moved appreciably between the measurements, such that errors between the cone-intersection values and actual spin axis orientations are due primarily to errors in sensor measurement and telemetry accuracy.

Finally, if a third sensor is available, then a third sensor angle implies a third cone intersection at *one* of the two previously described cone-intersection loci. This provides a unique solution of the spin axis. However, in actual cases, the three cones do not intersect at a common locus, but at three close intersections (figure 3). Again, this effect is due to errors.

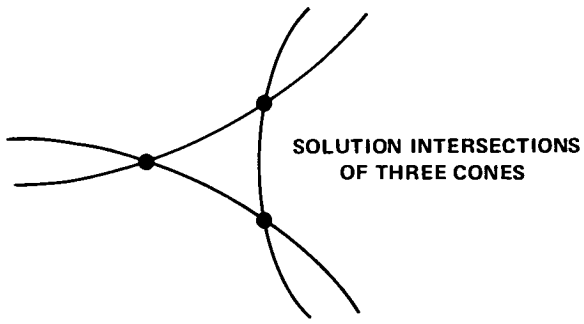

Figure 3. Effect of Errors on Cone Intersections

Cross Axis Determination

The cross axis is any axis perpendicular to the spin axis; thus, in the above definition of spin-stabilized spacecraft attitude, the spin axis is the spacecraft z-axis and the cross axis is either the x-axis or the y-axis. The cross axis is determined by specifying the rotation around the z-axis which brings the cross axis into a known reference plane; for example, rotation around z by θ bringing x into the Zz plane.

To provide known reference-plane/cross-axis relations for the spinning satellite requires sensors for observation of external objects or fields, such as the sun or the magnetic field of the earth, an internal spacecraft-relative clock or counter of known rate, a means of relating the clock to universal time, and the angles from the cross axis to the sensors. These requirements serve to relate the cross axis to a direction in space at a particular spacecraft-relative time, which corresponds to a particular instant of universal time.

As an example, consider a spacecraft with a sun sensor (see Appendix B), constant rate counters, and associated electronics and telemetry systems. The information for cross axis determination is produced through the following procedure:

1. The angle θ_0 between the cross axis and the sun-sensor/spin-axis plane is constructed according to the spacecraft design.

2. The spin period T is derived from the number of counts between sequential sightings of the sun by the sun sensor.

3. The number of counts between the transmitting of a particular telemetry word and the first sun sighting gives the relative time Δt_1 between those events by t_1 = counts/count rate.

4. The universal time, t_u, of the transmission of the particular telemetry word is computed from the known universal time at the receiving station and the propagation time delay from the satellite at known range to the receiving station, Thence,

5. The universal time of the first sun sighting is

$$t_s = t_u + \Delta t_1$$

for which time the inertial coordinates of the sun are known.

6. At time t_s, the angle θ in the xy plane between the cross axis and the known reference plane is simply the engineered spacecraft angle, $\theta = \theta_0$.

7. At a somewhat later time, $t_a = t_s + \Delta t_2$, the angle is given by

$$\theta = \theta_0 + \frac{t_2}{T} \times 360^\circ .$$

The final transformation of the cross axis into inertial coordinates depends on the instantaneous position of the sun at time t_s in inertial coordinates, and the orientation of the spin axis with respect to solar coordinates at time t_s, but this initial step in spin-stabilized spacecraft attitude determination is made preliminary to and independent of knowledge of the spin axis orientation.

SOME NON-LEAST SQUARES METHODS OF SOLUTION

The Unique Solution, Three-constraint (PQV) Approach

If a spacecraft has two cone angle sensors, then at some time t_i, two vectors, $\vec{P}_i$ and $\vec{Q}_i$, are known, and their associated cone angles, β_i and δ_i, are measured. The spin axis vector $\vec{S}$ (spacecraft z-axis) is unknown, but is related to the known quantities by the dot products

$$\hat{P}_i \cdot \hat{S} = \cos\beta_i = P_{X_i} S_X + P_{Y_i} S_Y + P_{Z_i} S_Z$$

and

$$\hat{Q}_i \cdot \hat{S} = \cos\delta_i = Q_{X_i} S_X + Q_{Y_i} S_Y + Q_{Z_i} S_Z$$

where $\hat{P}_i$, $\hat{Q}_i$, and $\hat{S}$ are unit vectors in the XYZ coordinate system. The three spin axis components—S_x, S_y, and S_z—are unknown; hence, they cannot be explicitly solved for by just these two equations. A third equation in S_x, S_y, and S_z is available, however, by virtue of $\hat{S}$ being a unit vector; that is,

$$S_X^2 + S_Y^2 + S_Z^2 = 1.$$

This introduction of a quadratic equation leads to a two-solution ambiguity as required for the two-cone intersection case. The quadratic approach is algebraically tedious, but a third linear equation can be formed which gives a more elegant set of equations for a solution. See figure 4.

A third vector, $\vec{V}_i$, perpendicular to $\vec{P}_i$ and $\vec{Q}_i$, is defined as the cross product of $\hat{P}_i$ and $\hat{Q}_i$

$$\vec{V}_i \equiv \hat{P}_i \times \hat{Q}_i = \sin\eta_i \hat{V}_i$$

where $\hat{V}_i$ is the unit vector. Then,

$$\hat{V}_i = \frac{\hat{P}_i \times \hat{Q}_i}{\sin\eta_i}$$

with components,

$$V_{X_i} = \frac{P_{Y_i}Q_{Z_i} - P_{Z_i}Q_{Y_i}}{\sin \eta_i} \; ; \; V_{Y_i} = \frac{P_{Z_i}Q_{X_i} - P_{X_i}Q_{Z_i}}{\sin \eta_i} \; ; \; V_{Z_i} = \frac{P_{X_i}Q_{Y_i} - P_{Y_i}Q_{X_i}}{\sin \eta_i}$$

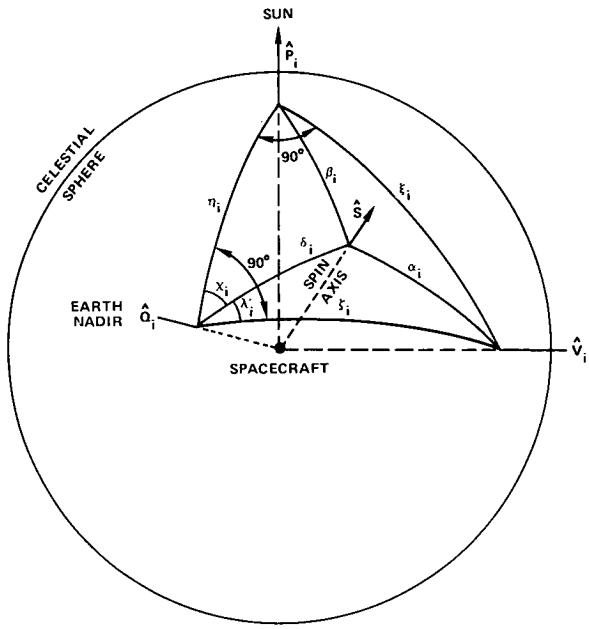

Figure 4. Spin Axis, $\hat{S}$, Related to Known Axes $\hat{P}_i$, $\hat{Q}_i$, $\hat{V}_i$

The angle η_i between $\hat{P}_i$ and $\hat{Q}_i$ is also given by

$$\hat{P}_i \cdot \hat{Q}_i = \cos \eta_i \, .$$

The relation needed to define the cone angle α_i between the new vector $\hat{V}_i$ and the spin axis vector $\hat{S}$ is the dot product

$$\hat{V}_i \cdot \hat{S} = \cos \alpha_i = V_{X_i}S_X + V_{Y_i}S_Y + V_{Z_i}S_Z \, .$$

Thus, to solve the three dot-product equations involving $\hat{S}$ for the three components S_X, S_Y, and S_Z requires the evaluation of α_i. By the use of the law of cosines from spherical trigonometry applied to figure 4 and the observation that ξ_i and ζ_i equal 90°, the auxiliary angles χ_i and λ_i are determined. From the law of cosines

$$\cos \chi_i = \frac{\cos \beta_i - \cos \eta_i \cos \delta_i}{\sin \eta_i \sin \delta_i}$$

and

$$\lambda_i = 90^\circ - \chi_i \Rightarrow \cos\lambda_i = \cos(90^\circ - \chi_i) = \sin\chi_i .$$

The desired angle α_i now follows, by the law of cosines:

$$\cos\alpha_i = \cos\delta_i \cos\zeta_i = \sin\delta_i \sin\zeta_i \cos\lambda_i = \sin\delta_i \cos\lambda_i = \sin\delta_i \sin\chi_i .$$

There are now three equations and three unknowns:

$$\cos\beta_i = P_{X_i} S_X + P_{Y_i} S_Y + P_{Z_i} S_Z$$

$$\cos\delta_i = Q_{X_i} S_X + Q_{Y_i} S_Y + Q_{Z_i} S_Z$$

$$\cos\alpha_i = V_{X_i} S_X + V_{Y_i} S_Y + V_{Z_i} S_Z$$

or in matrix notation

$$[C]_i = \begin{bmatrix} P_{X_i} & P_{Y_i} & P_{Z_i} \\ Q_{X_i} & Q_{Y_i} & Q_{Z_i} \\ V_{X_i} & V_{Y_i} & V_{Z_i} \end{bmatrix} \begin{bmatrix} S_X \\ S_Y \\ S_Z \end{bmatrix} = [PQV]_i [S].$$

Unless $\hat{P}$ is parallel to $\hat{Q}$, [PQV] is nonsingular and possesses an inverse such that the solution of [S] is

$$[S] = [PQV]_i^{-1} [C]_i .$$

The question arises as to what happens to the ambiguity in the initial two-cone-angle solution. The choice of the order of $\hat{P}$ and $\hat{Q}$ in the cross product makes a difference in the sign of $\vec{V}$. Thus, if $\hat{P} \times \hat{Q} = \vec{V}$, then $\hat{Q} \times \hat{P} = -\vec{V}$, and the resultant [S] matrix components from using $-\vec{V}$ in [PQV] are the expected second solutions. From these vector relations and knowledge of the spin period, the time between separate sensor sightings, and the angle between the two sensors, an unambiguous method of selecting the correct solution is possible. This method and appropriate tests are described in Appendix C.

If the time between sensor sightings is not available, as is the case with magnetometers, many sets of equations can be formed corresponding to different conditions at different times t_i, with each set of equations providing two solutions as outlined above. From each pair of solutions, one is closest to previous solutions or *a priori* expectations of the spin axis vector, and is chosen for the set of all best solutions. These best solutions will be reasonably close in value, but will differ even for solutions of a stationary spin axis vector.

The errors which propagate to create the solution discrepancies are due (1) to engineering limitations (for example, half-degree accuracy of the sun sensor, three quarters of a degree accuracy for an earth sensor, and angle uncertainties related to the digital counter); (2) to field model uncertainties; (3) to spacecraft, sun, and other position vector uncertainties; and (4) to random errors at each stage of the procedure. The systematic errors can be lessened by various long-period, observation-deduced adjustments, but there are always residual random deviations.

Three-constraint Solution Applied to IMP-6

IMP-6 is the sixth in the series of Interplanetary Monitoring Platforms. It has a highly elliptical orbit about the earth (perigee of approximately 12,000 km and apogee of approximately 210,000 km), and is primarily engaged in investigation of the earth's magnetic field. For attitude determination, it possesses an earth horizon sensor and a sun sensor.

The PQV method for IMP-6 attitude determination makes use of the satellite's earth horizon and sun sensors to derive cone angles. The derivations of the earth nadir cone angle δ depend on the earth-spacecraft-sun relations, with two cases favorable for cone angles. Case 1 is involved when the earth sensor detects two earth horizons in a single sweep across the visible earth. Case 2 applies when one horizon and one terminator are detected.

The sensors operate generally as described in Appendix B. Specifically, a 9-bit sun sensor gives 0.5° accuracy in the sun angle, β; a 1.5° horizon sensor field of view gives a 0.75° apparent increase in the earth radius; and a 1600 counts-per-second oscillator drives the counters and thus provides resolutions of 0.000625 s between counts. The counters are a sun clock measuring the time between a specific bit of the telemetry format and the next sun pulse, a spin-period counter measuring the time between successive sun pulses, a sun-earth horizon counter measuring the time between a sun pulse and the next initial sensing of the earth, and an earth-width counter, which measures the scan time between initial earth horizon detection and the trailing earth horizon. The mounting angle γ (figure 5) between spin axis and earth sensor is 87°, off by 3° from the desired 90°.

The presence of a terminator, rather than an earth horizon, as either the initial or trailing counter trigger is determined analytically. From the sun-earth horizon counter, EI (Earth IN), and the spin period counter, SPC, the angle ν between the spin axis/sun plane and the spin axis/earth horizon plane is found by

$$\text{EIT} = \text{EI counts} \times 0.000625 \text{ seconds/count}$$

$$\text{SP} = \text{SPC counts} \times 0.000625 \text{ seconds/count}$$

$$\frac{\nu}{360} = \frac{\text{EIT}}{\text{SP}} \quad \text{or} \quad \nu = 360^\circ \times \frac{\text{EIT}}{\text{SP}}$$

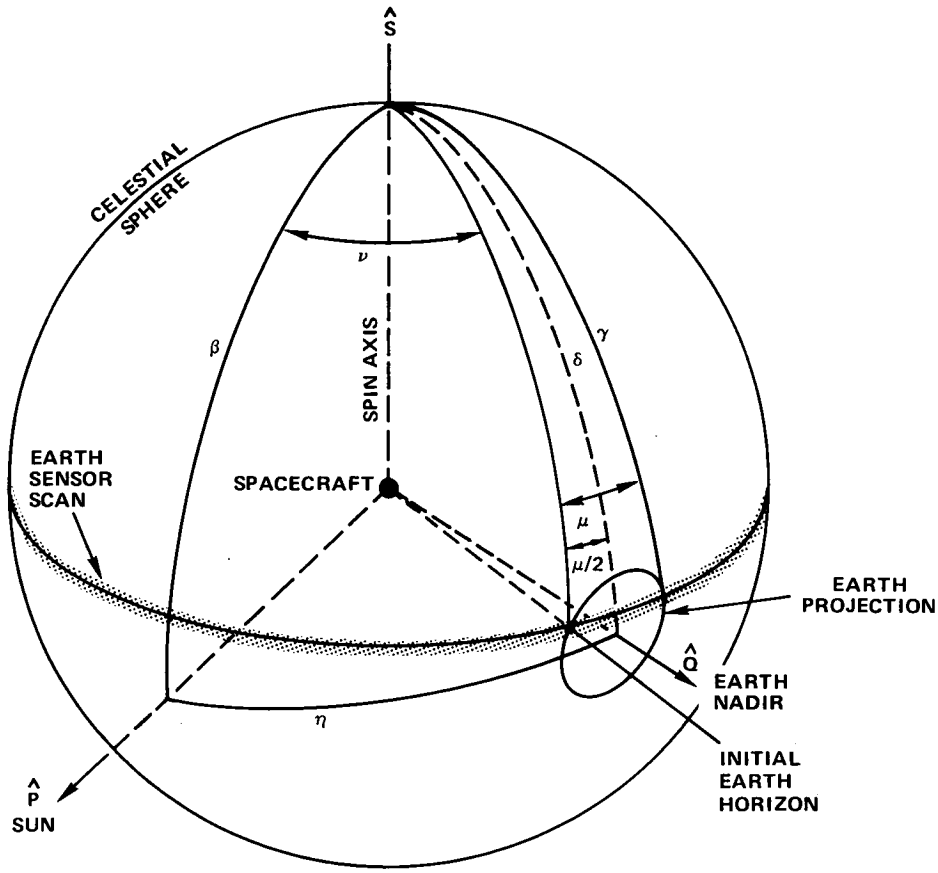

Figure 5. Vectors and Related Angles

where EIT = Earth In Time,

EI = Earth In,

SP = Spin Period,

SPC = Spin Period Counter.

If $0 < \nu < 180°$, initial earth detection is at the earth horizon, because of the sunlight-on-earth illumination geometry. The angle 2ρ subtended by the earth at the spacecraft distance is derived from $\sin \rho = R_e/(R_e + h)$, where R_e is the earth radius (see figure 6a) and h is the spacecraft altitude.

The angle ϕ between the spacecraft position vector and the sun vector is defined by $\hat{P} \cdot (-\hat{Q}) = \cos \phi$ or by

$$\phi = 180° - (\nu + \rho) \quad \text{for } 0 < \nu + \rho < 180°$$

$$\phi = (\nu + \rho) - 180° \quad \text{for } 180° < \nu + \rho < 360°.$$

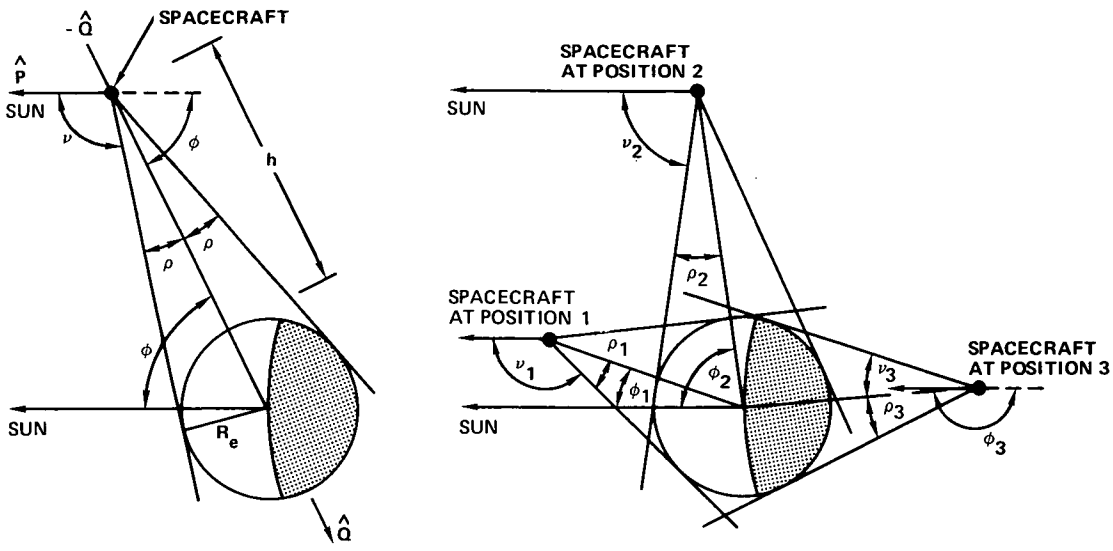

(a) Angle and Vector Relations

(b) Spacecraft in Three Positions

Figure 6. Relation of Spacecraft to Sunlit and Shadowed Earth

Then, for $\phi \leq \rho$, as for the spacecraft in position 1 in figure 6b, the spacecraft views a fully sunlit earth, and the earth sensor senses two earth horizons. But for $\phi > \rho$ and $\nu > 0$, with the spacecraft in position 2, the spacecraft senses an earth horizon and a terminator. When $\nu = 0$, with the spacecraft in position 3, then either the earth horizon sensor does not scan the earth or the earth viewed by the sensor is entirely shadowed.

With these criteria established, the earth nadir angle, δ, can be derived according to one of the two cases mentioned above.

Case 1—Nadir Angle Derivation for Scan of Two Horizons—In the event that $\phi \leq \rho$ (figure 6b, spacecraft at position 1), a scan from horizon to horizon by the earth horizon sensor (figure 7) provides a measure of an arc, μ, across the earth. Half of the angle μ is the angle $\mu/2$ between the spin axis–earth horizon plane and the spin axis–earth center plane. By the law of cosines,

$$\cos \rho = \cos \gamma \cos \delta + \sin \gamma \sin \delta \cos \frac{\mu}{2} ,$$

and by

$$\cos^2 \delta + \sin^2 \delta = 1$$

the equation can be solved. Another linear relation exists, however, and can be used rather than the quadratic:

$$\cos \eta = \cos \beta \cos \delta + \sin \beta \sin \delta \cos \left(\nu + \frac{\mu}{2}\right) .$$

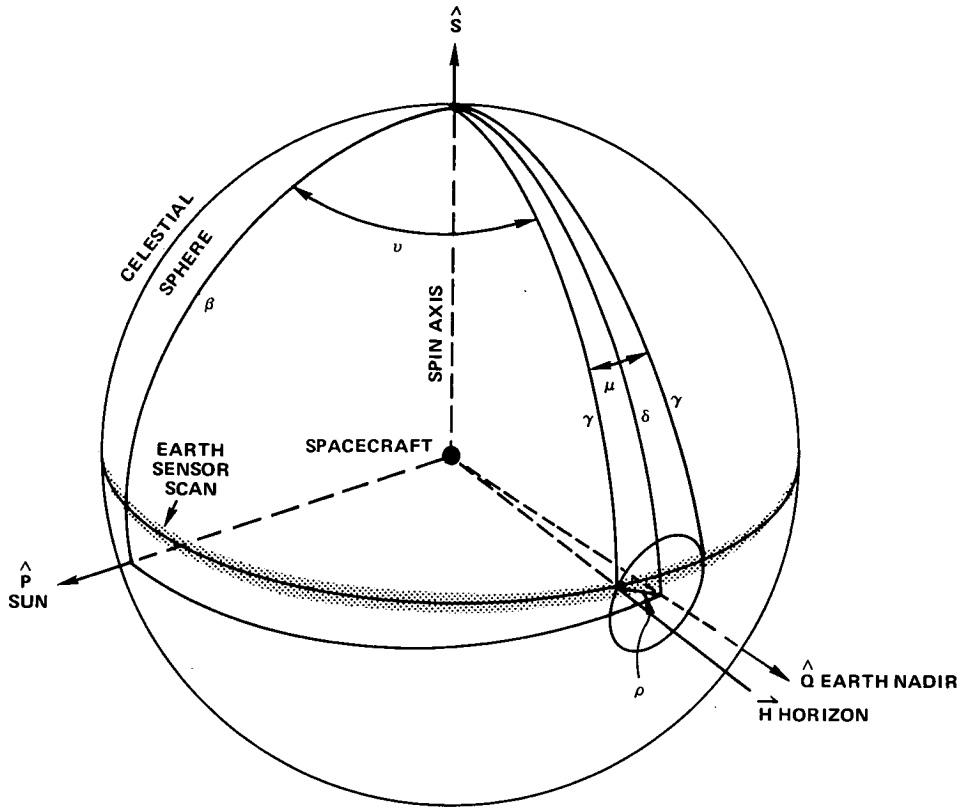

Figure 7. Case 1, Nadir Angle Derivation, Scan of Two Horizons

The cos η and cos ρ equations can be viewed as two equations in the two unknowns, cos δ and sin δ, and solved accordingly:

$$\cos\delta = \frac{\cos\rho - \sin\gamma \sin\delta \cos\frac{\mu}{2}}{\cos\gamma}$$

such that

$$\cos\eta\cos\gamma - \cos\gamma\sin\beta\sin\delta\cos\left(\nu+\frac{\mu}{2}\right) = \left(\cos\rho - \sin\gamma\sin\delta\cos\frac{\mu}{2}\right)\cos\beta\sin\delta$$

$$\left[\cos\beta\sin\gamma\cos\frac{\mu}{2} - \cos\gamma\sin\beta\cos\left(\nu+\frac{\mu}{2}\right)\right] = \cos\rho\cos\beta - \cos\eta\cos\gamma\sin\delta$$

$$= \frac{\cos\beta\cos\rho - \cos\eta\cos\gamma}{\cos\beta\sin\gamma\cos\frac{\mu}{2} - \cos\gamma\sin\beta\cos\left(\nu+\frac{\mu}{2}\right)}.$$

All angles on the right-hand side of the equation are determined from spacecraft measurements (β, ν, and $\mu/2$), from orbit determination (ρ and η), and from spacecraft engineering, (the mounting angle of the horizon sensor γ), allowing δ to be computed.

Case 2—Nadir Angle Derivation for Scan of One Horizon and the Earth Terminator—In the event that $\phi > \rho$ and $\nu > 0$, no useful information is acquired from the earth horizon sensor scan from an earth horizon to the earth terminator (figure 8). The angle μ merely provides an angle that is less than the full arc across the earth. Elaborate geometrical and trigonometric analysis could supply a proportionate angle equivalent to $\mu/2$, but a simpler approach is available.

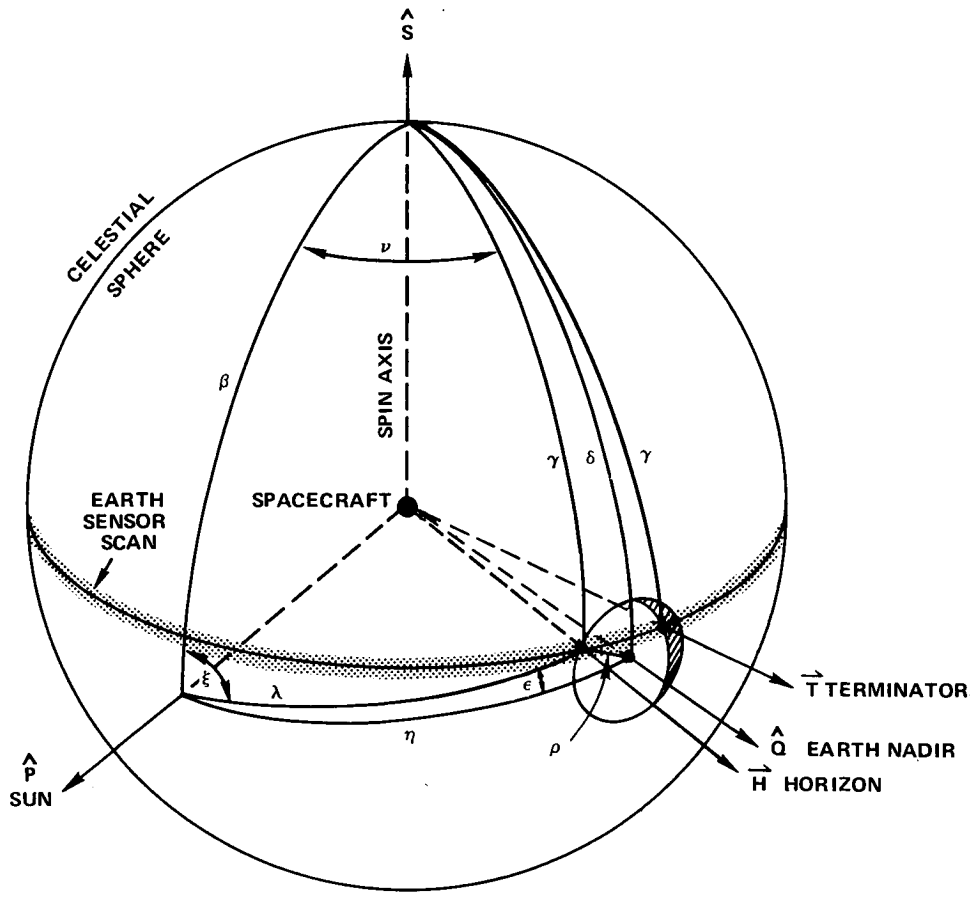

Figure 8. Case 2, Nadir Angle Derivation, Scan of One Horizon and Earth Terminator ($\gamma < \delta$)

The great circle arc λ, between the sun position vector $\hat{P}$ and the earth horizon vector $\vec{H}$, is found by use of the law of cosines,

$$\cos \lambda = \cos \beta \cos \gamma + \sin \beta \sin \gamma \cos \nu .$$

The interior angle ξ results from an application of the law of sines,

$$\sin \xi = \sin \gamma \frac{\sin \nu}{\sin \lambda} .$$

The last auxiliary angle, the interior angle ϵ, is also given by the law of cosines:

$$\cos \epsilon = \frac{\cos \rho - \cos \lambda \cos \eta}{\sin \lambda \sin \eta}$$

Then,

$$\cos \delta = \cos \beta \cos \eta + \sin \beta \sin \eta \cos (\xi + \epsilon)$$

for $\gamma < \delta$ and

$$\cos \delta = \cos \beta \cos \eta + \sin \beta \sin \eta \cos (\xi - \epsilon)$$

for $\gamma > \delta$ (figure 9). But since δ is not known beforehand in relation to γ, a two-value ambiguity in δ results.

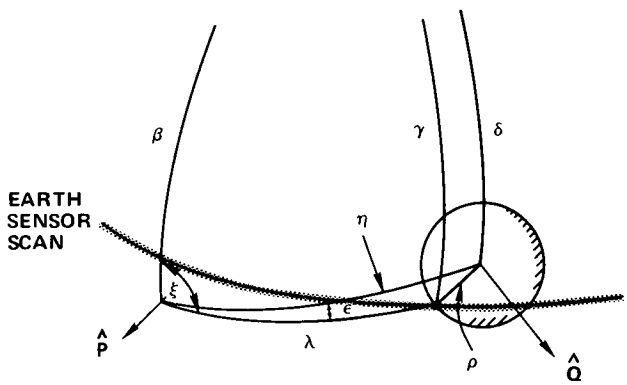

Figure 9. Case 2, Nadir Angle Derivation, Scan of One Horizon and Earth Terminator ($\gamma > \delta$)

Various other angles can be developed and applied as criteria to the selection of allowable data for the solution of δ. (For this more extensive and complete treatment of the PQV method see reference 3.)

One other augmentation of the above equations is necessary for completeness. If the terminator is sensed first by the earth scanner, and an earth horizon triggers the trailing pulse, then in each of the equations for case 2 where ν is present, the substitution $\nu + \mu$ is made.

A relation mentioned above in another context also provides the specifications for the order of the horizon and terminator. If $0 < \nu + \rho < 180°$, an earth horizon is sensed prior to the terminator. If $180° < \nu + \rho < 360°$, the earth terminator preceeds the horizon. For $\nu + \rho$ angles near 180° (dependent on the radial distance of the spacecraft from the earth), the spacecraft views a fully sunlit earth.

By these means the required cone angles β and δ are acquired for the solution of the IMP-6 spin axis orientation. The solution itself follows the algorithm outlined above with the additional ambiguity in δ in the horizon/terminator case leading to a four-way ambiguity in the spin-axis solution (two δ's for each cone intersection).

An adjustment of the θ and μ angles must be made in practice in order to eliminate the systematic error reducing the counts caused by the 1.5° field of view of the telescope. This adjustment is discussed in the last paragraphs of "Spherical Coordinate Solutions Applied to IMP-6," below.

The Unique Solution, Spherical Coordinates (Right Ascension and Declination) Approach

A more general treatment of the spin-stabilized spacecraft attitude problem focuses on the long-term, inertially-constant axis of rotation. This axis, the net angular momentum vector $\hat{L}$, is not, in general, the instantaneous spin axis $\hat{S}$. Except for the special case where the principal moment of inertia I_z of the z-axis is greater than the transverse principal moments of inertia I_x and I_y, the angle between the two moments at which the spin axis precesses about the momentum vector tends to zero (unless the symmetry axes and principal moment axes are misaligned). This is the nominal condition of most spin-stabilized spacecraft, and the following discussion makes reference to the momentum vector, rather than to the spin axis, in accordance with existing literature* on the method (reference 4).

Figure 10 is a representation of the celestial sphere centered at the spacecraft center of mass with all vectors emanating from that point. The components of the vectors are in spherical coordinates with respect to the equatorial, inertial reference system defined by Z = celestial north, X = first point of Aries, and Y = orthogonal axis making a right-handed

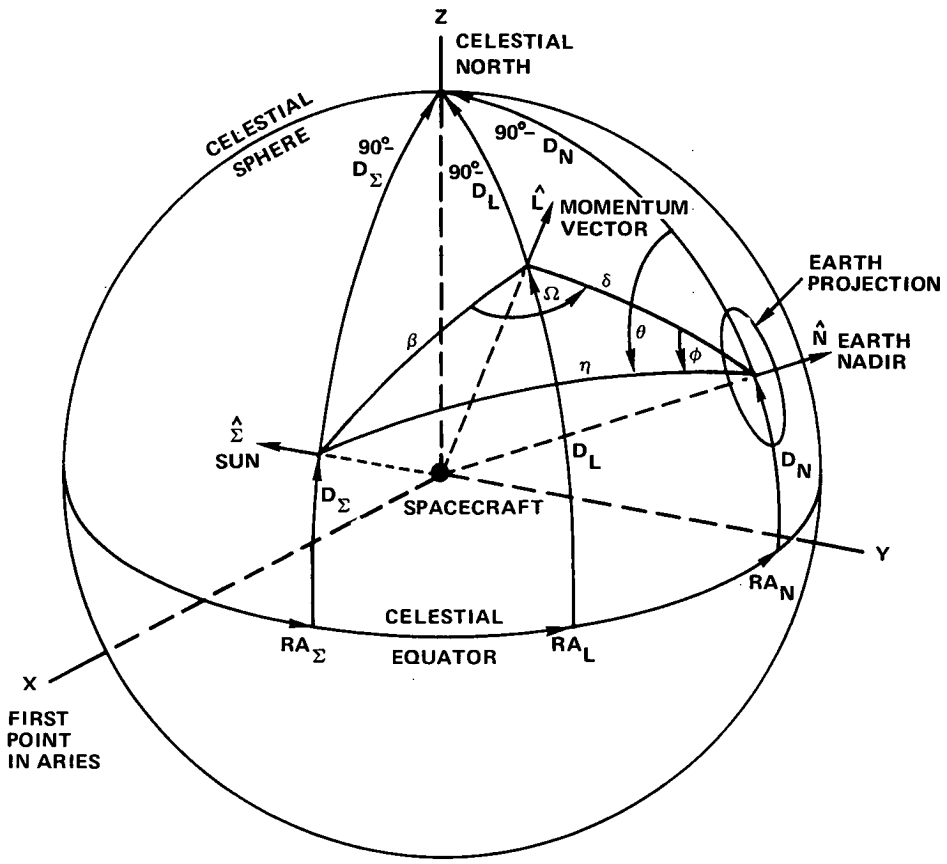

Figure 10. Right Ascension and Declination Components of Earth, Sun, and Momentum Vectors

*Pyle, E. J. and J. S. Albus, *IMP F & G Aspect Determination System*, GSFC X-711-67-30 (TM X-63526), January 1967.

system. The spherical components of a unit vector $\hat{V}$ are the right ascension RA_v and the declination D_v. The vectors shown are the sun position, earth nadir, and angular momentum unit vectors, $\hat{\Sigma}$, $\hat{N}$, and $\hat{L}$, respectively. The arcs of the great circles between the vectors are β between $\hat{\Sigma}$ and $\hat{L}$, η between $\hat{\Sigma}$ and $\hat{N}$, and δ between $\hat{L}$ and $\hat{N}$.

As discussed in the section, "The Unique Solution, Three-Constraint (PQV) Approach," the angles β and δ are determined from spacecraft observations, $\hat{\Sigma}$ is the sun position at the time of the observations, $\hat{N}$ is the negative vector of the spacecraft orbital position, and η is the arccosine of the dot product of $\hat{\Sigma}$ and $\hat{N}$. From these known quantities, the angular momentum components, RA_L and D_L, can be derived. Explicitly, use is made of the spherical coordinates, RA_Σ, D_Σ, RA_N, and D_N, the angles δ, β, and η, various auxiliary interior angles, and the spherical trigonometric laws of sines and cosines in the following equations to obtain the required relations.

Let the auxiliary interior angle ϕ be formed by the ccw rotation of the δ arc into the η arc around $\hat{N}$. The angle is defined by the law of cosines relation

$$\cos\phi = \frac{\cos\beta - \cos\eta\cos\delta}{\sin\eta\sin\delta}$$

Similarly, the auxiliary interior angle between $(90^\circ - D_N)$ and η is formed by

$$\cos\theta = \frac{\cos(90^\circ - D_\Sigma) - \cos(90^\circ - D_N)\cos\eta}{\sin(90^\circ - D_N)\sin\eta} = \frac{\sin D_\Sigma - \sin D_N\cos\eta}{\cos D_N\sin\eta} .$$

The difference angle $(\theta - \phi)$ is used to define the D_L relations,

$$\cos(90^\circ - D_L) = \cos(90^\circ - D_N)\cos\delta + \sin(90^\circ - D_N)\sin\delta\cos(\theta - \phi)$$

and

$$\sin D_L = \sin D_N\cos\delta + \cos D_N\sin\delta\cos(\theta - \phi) \quad (-90^\circ < D_L \leqslant 90^\circ).$$

NOTE: If η is between δ and $(90^\circ - D_N)$, then ϕ becomes a negative angle by the defining convention. Sign considerations must be implemented on the D_L equation for full generality. This is done by using the additional defining equations of ϕ and θ to provide the quadrant of each angle.

A second ϕ relation is

$$\sin\phi = \sin\beta\,\frac{\sin\Omega}{\sin\eta}$$

where Ω is the interior angle about $\hat{L}$ from the $\hat{\Sigma}\,\hat{L}$ plane to the $\hat{N}\hat{L}$ plane. This angle is determined by sensor pulse-times, and will be discussed in the next section, "Spherical Coordinate Solutions Applied to IMP-6." The second θ relation is

$$\sin\theta = \sin(90^\circ - D_\Sigma)\frac{\sin(RA_N - RA_\Sigma)}{\sin\eta} = \cos D_\Sigma \frac{\sin(RA_N - RA_\Sigma)}{\sin\eta} .$$

Two relations are also required to define RA_L and its quadrant

$$\cos(RA_N - RA_L) = \frac{\cos\delta - \cos(90^\circ - D_N)\cos(90^\circ - D_L)}{\sin(90^\circ - D_N)\sin(90^\circ - D_L)} = \frac{\cos\delta - \sin D_N \sin D_L}{\cos D_N \cos D_L}$$

and

$$\sin(RA_N - RA_L) = \sin\delta \frac{\sin(\theta - \phi)}{\sin(90^\circ - D_L)} = \sin\delta \frac{\sin(\theta - \phi)}{\cos D_L} .$$

Since RA_N is known,

$$RA_L = RA_N - (RA_N - RA_L) .$$

The parameters given in the section, "The Unique Solution, Three-Constraint (PQV) Approach," are equivalent to those of this section by

$$\hat{P} \Leftrightarrow \hat{\Sigma}$$
$$\hat{Q} \Leftrightarrow \hat{N}$$
$$\hat{S} \Leftrightarrow \hat{L}$$

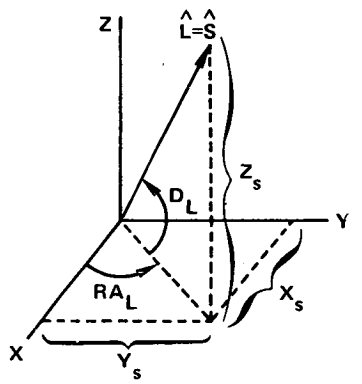

Figure 11. Right Ascension, Declination and XYZ Components of $\hat{L}$

and the spherical coordinate components of $\hat{L}$, as shown in figure 11, are related to the Cartesian coordinate components of $\hat{S}$ by

$$X_s = \cos D_L \sin RA_L$$

$$Y_s = \cos D_L \cos RA_L$$

$$Z_s = \sin D_L .$$

Spherical Coordinate Solutions Applied to IMP-6

The application of the RA and D method to the IMP-6 satellite obviously entails the use of the same telemetry information produced by the same engineering design described above in the section, "Three-constraint Solution Applied to IMP-6." However, different algorithms for the determination of the angle δ between the $\hat{L}$ and $\hat{N}$ vectors were incorporated in the actual RA and D method attitude determination program. Accordingly, these algorithms and the pertinent spacecraft observations are briefly examined below.

First, consider case 1 for which two earth horizons are scanned. In this case, the angle μ between the horizons is determined from the earth width counter, and the angle ν between the $\hat{\Sigma}\hat{L}$ plane and the $\hat{L}\hat{H}_1$ plane is determined from the sun-earth counter. The angle $\mu/2$ between the $\hat{L}\hat{H}_1$ plane and the $\hat{L}\hat{N}$ plane provides the final angle necessary to form the interior angle Ω of the previous section, $\Omega = \nu + \mu/2$ (figure 12).

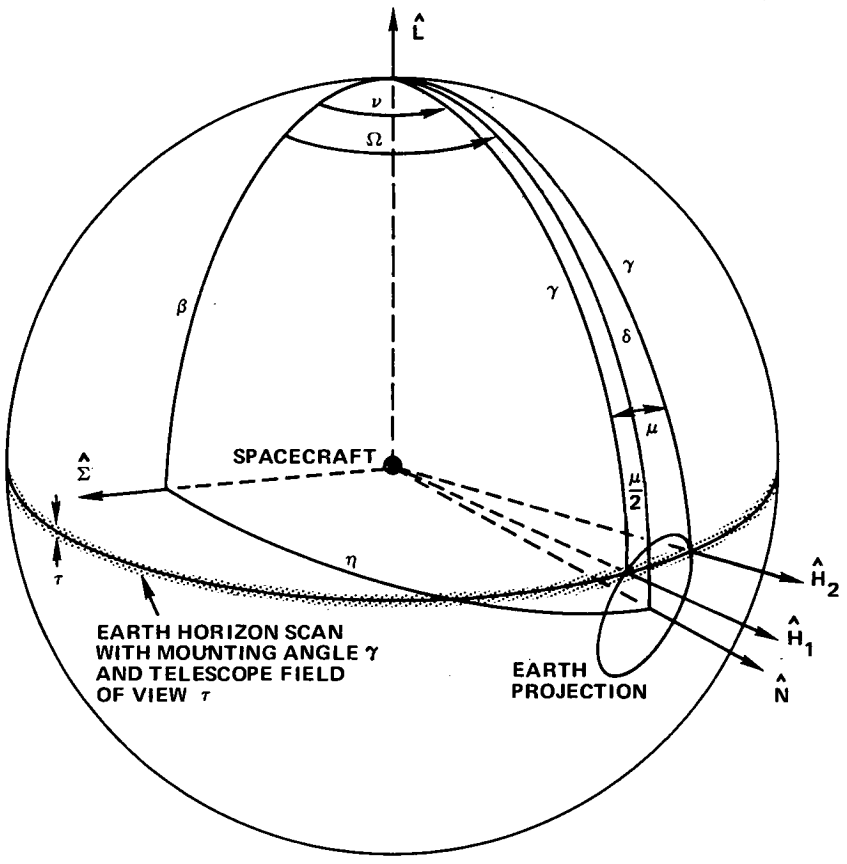

Figure 12. Case 1, Two Earth Horizons Scanned

By the law of cosines,

$$\cos\eta = \cos\beta\cos\delta + \sin\beta\sin\delta\cos\Omega$$

and by

$$\sin\delta = \sqrt{1 - \cos^2\delta}, \quad \cos\eta - \cos\beta\cos\delta = \sin\beta\cos\Omega\sqrt{1 - \cos^2\delta}\ .$$

Squaring both sides and collecting terms of order $\cos\delta$,

$$(\cos^2\beta + \sin^2\beta\cos^2\Omega)\cos^2\delta - (2\cos\eta\cos\beta)\cos\delta + (\cos^2\eta - \sin^2\beta\cos^2\Omega) = 0.$$

By the quadratic formula,

$$\cos\delta = \frac{2\cos\eta\cos\beta \pm \sqrt{4\cos^2\eta\cos^2\beta - 4(\cos^2\beta + \sin^2\beta\cos^2\Omega)(\cos^2\eta - \sin^2\beta\cos^2\Omega)}}{2(\cos^2\beta + \sin^2\beta\cos^2\Omega)}$$

which simplifies to

$$\cos\delta = \frac{2\cos\eta\cos\beta \pm \sin\beta\cos\Omega\sqrt{\cos^2\beta + \sin^2\beta\cos^2\Omega - \cos^2\eta}}{\cos^2\beta + \sin^2\beta\cos^2\Omega}.$$

This two-solution ambiguity in δ is resolved by consideration of whether the angle δ should be less than or greater than the mounting angle γ of the sensor with respect to the spin axis.

Next, consider case 2 for which one earth horizon and the earth terminator are scanned (figures 13, 14). The items of significance in this case are the angles β, η, γ, ν, and ρ, all defined previously, and the auxiliary angles, λ, B, D, and E, derived from the known. The terminator/scan intersection $\hat{T}$ provides no information applicable to this derivation.

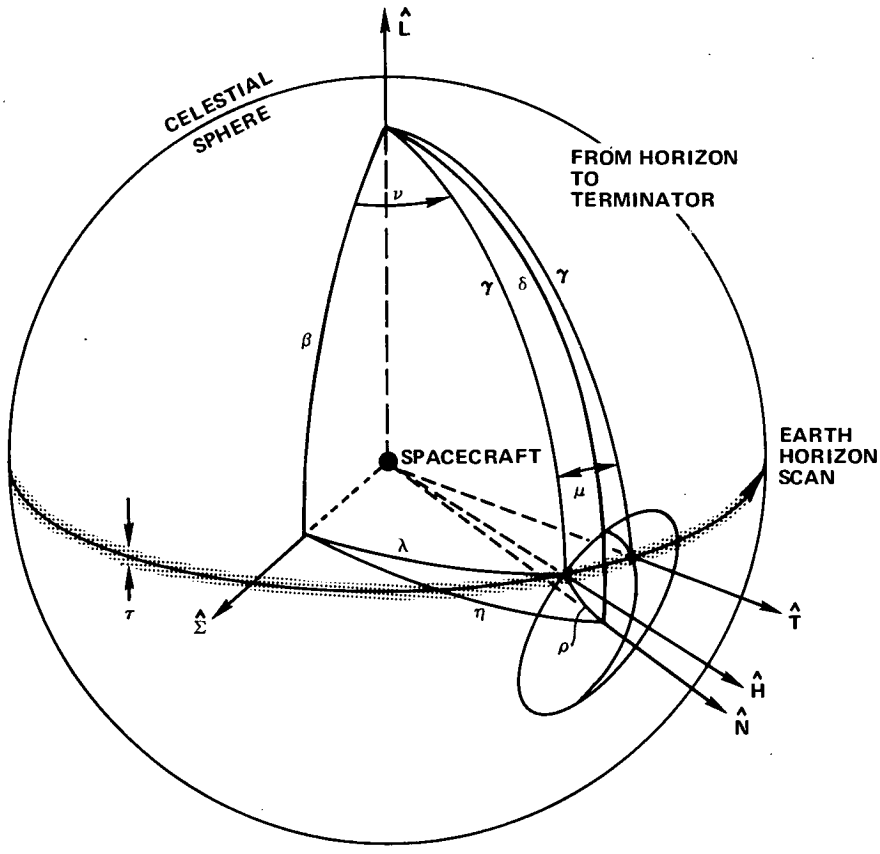

Figure 13. Case 2, Earth Horizon and Earth Terminator Scanned

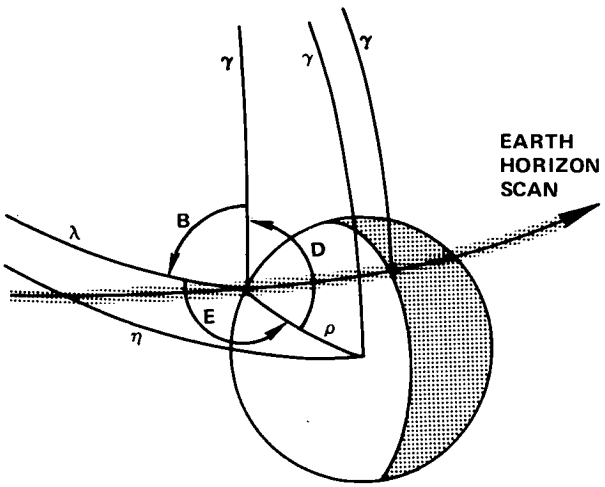

Figure 14. Earth Horizon and Earth Terminator Scanned (Detail of Figure 13).

From the law of cosines,

$$\cos\lambda = \cos\beta\cos\gamma + \sin\beta\sin\gamma\cos\nu$$

which holds for $0° < \nu < 180°$.

For $\nu > 180°$, the terminator is scanned first and the horizon, second, requiring ν to be replaced by $\mu + \nu$ in the equation. If $\nu = 180°$, then $\lambda = \beta + \gamma$. For this case, ν is the angle determined by the spacecraft counter which is triggered by the sun and shut off by an earth horizon/terminator scan, and μ is derived from the counter which is triggered by the horizon/terminator and shut off by the terminator/horizon.

The interior angles B, D, and E follow from the application of the laws of sines and cosines.

$$\cos B = \frac{\cos\beta - \cos\gamma\cos\lambda}{\sin\gamma\sin\lambda}$$

and

$$\sin B = \sin\beta\,\frac{\sin\nu}{\sin\lambda}\,.$$

For the interior angle E, two equations are not available to define the angle and its quadrant; so, a two-possible-values cosine equation produces an ambiguity in E,

$$\cos E = \frac{\cos\eta - \cos\lambda\cos\rho}{\sin\lambda\sin\rho},$$

where E can be in either of two quadrants. As a result, there are two possible values of D determined by

$$D = 360° - B - E$$

and the defining equation for δ in this case propagates a two-value ambiguity,

$$\cos\delta = \cos\rho\cos\gamma + \sin\rho\sin\gamma\cos D,$$

where δ in either of two quadrants satisfies.

The desired orientation for IMP-6 at the time of launch was for $RA_L = 90°$, $D_L = -66.5$, and a spin period of 11 seconds. After a series of maneuvers, from launch on March 13, 1971, through July 15, 1971, the satellite was permitted to remain in a spin-stabilized,

spin-axis orientation of about $RA_L = 95°$, $D_L = -67.5$, and a spin period of 12.8 seconds. In the course of determining the definitive attitude, an apparent coning of the spin axis about a separated momentum vector was not a necessary hypothesis if an assumption was made that the earth horizon sensor mounting angle γ was 87° rather than the desired, engineered 90°.

Another value adjusted to bring all solutions over an orbit into closer relative agreement was the angular earth radius ρ. The reason for this adjustment is the triggering of the earth-horizon scan pulse before the center of the sensor reaches the horizon (figure 15). The approximate adjustment value is half the scan width τ, that is, the radius of the field of view of the sensor telescope. Thus, when a certain small percentage of the sensor field of view is covered by the sunlit earth, the first horizon pulse or the trailing pulse is initiated. This provides fewer counts to the sun-earth horizon counter and more counts to the earth width counter, in direct proportion to the adjustment in ρ. The best value for the adjustment shifts according to the spacecraft distance to the earth, because the relative size of the earth with respect to the scan width varies, and the greater the curvature, the greater the proportion of the sensor which must cross the horizon to trigger the pulse (figure 16).

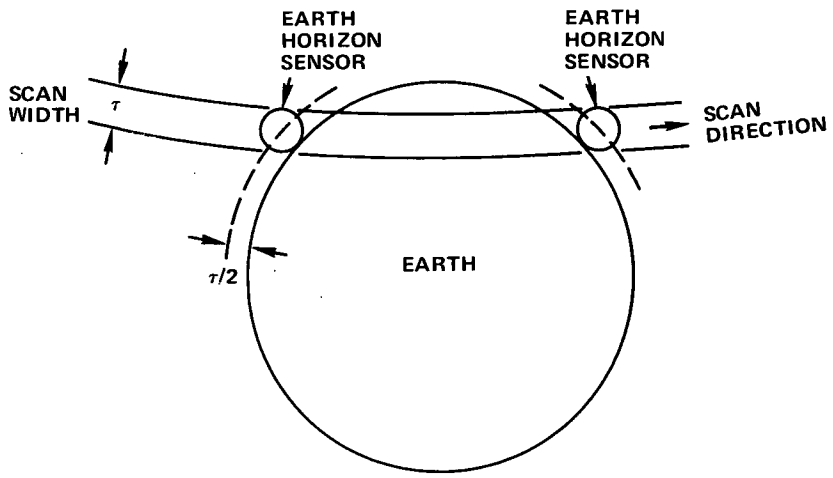

Figure 15. Earth Horizon Sensor at Times of Scan Pulses

For IMP-6, with a nominal scan width 1.5, the adjustment value near perigee has been 0.8 and the value near apogee, 0.6. The chosen adjustment value affects only those equations with ρ related to counter-derived values.

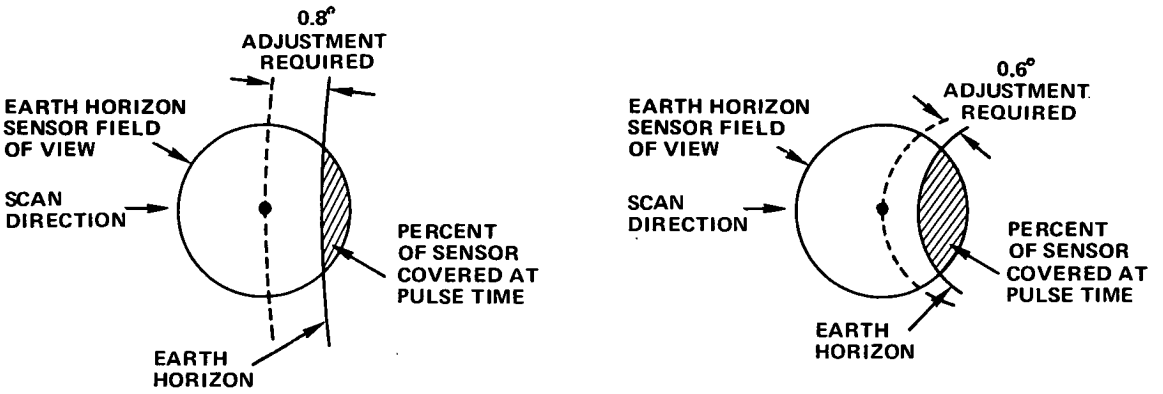

Figure 16. Different Adjustments of Angular Earth Radius ρ with Constant Percentage of Sensor Covered

LEAST SQUARES METHODS OF SOLUTION

The Iterative Differential Correction Technique

In a typical spin-stabilized spacecraft attitude determination system an abundance of cone intersection pairs are produced over a relatively short time by the spacecraft sensors. To make use of all of them, the method of least squares is applied to solve the over-determined set of equations. See Appendix D for a brief description of the method of least squares.

If the equations involve spherical coordinates, and are to be solved for the angular attitude components RA_L and D_L, then the equations are not linear and a closed form solution in RA_L and D_L is not practical. Instead, a series of small corrections to successive, iterated values of RA_L and D_L are produced, until the size of corrections are less than preselected small amounts.

Each set of solution correction values is produced by a least squares treatment. The procedure is to expand the equations in a Taylor's series in terms of the required coordinates, truncate the series after the linear terms, solve the truncated equations by least squares for the correction values, apply the corrections to the last values of the components, and repeat the cycle until the newest corrections are less than the preselected bounds.

The form of the equations prior to expansion in terms of RA_L and D_L is, for n equations,

$$\hat{U}_i \cdot \hat{L} = \cos\theta_i = U_{X_i} \cos D_L \cos RA_L + U_{Y_i} \cos D_L + RA_L + U_{Z_i} \sin D_L$$

where $\hat{U}_i$ = the known unit vectors (sun, earth nadir, or magnetic field),

$\hat{L}$ = the spin axis (or angular momentum) unit vector,

θ_i = the cone angles (β, δ, and so on),

$U_{X_i}, U_{Y_i}, U_{Z_i}$ = the inertial coordinate components of $\hat{U}_i$, i = 1, . . . n, and

D_L and RA_L = the inertial, spherical coordinate components of $\hat{L}$, which are to be solved for.

The functional equation

$$F_i(RA_L, D_L) = \cos\theta_i - U_{X_i} \cos D_L \cos RA_L - U_{Y_i} \cos D_L \sin RA_L - U_{Z_i} \sin D_L = 0$$

is expanded in a Taylor's series about initial coordinates RA_L°, D_L° by

$$F_i(RA_L, D_L) = F_i(RA_L^\circ, D_L^\circ) + \left(\frac{\partial F_i}{\partial RA}\right)_0 \Delta RA_L + \left(\frac{\partial F_i}{\partial D_L}\right)_0 \Delta D_L + \left(\frac{\partial^2 F_i}{\partial RA^2}\right)_0 (\Delta RA)^2 + \ldots$$

and truncated after the $(\partial F_i/\partial D_L)_0 \Delta D_L$ term. For notational convenience let

$$\left(\frac{\partial F_i}{\partial RA_L}\right)_0 \equiv \frac{\partial F_i}{\partial RA_L^\circ}, \left(\frac{\partial F_i}{\partial D_L}\right)_0 \equiv \frac{\partial F_i}{\partial D_L^\circ},$$

then

$$F_i(RA_L, D_L) \approx F_i(RA_L^\circ, D_L^\circ) + \frac{\partial F_i}{\partial RA_L^\circ} \Delta RA_L + \frac{\partial F_i}{\partial D_L^\circ} \Delta D_L$$

where

$$F_i(RA_L^\circ, D_L^\circ) = \cos\theta_i - U_{X_i} \cos D_L^\circ \cos RA_L^\circ - U_{Y_i} \cos D_L^\circ \sin RA_L^\circ - U_{Z_i} \sin D_L^\circ = \rho_i^\circ$$

and the ρ_i° are the residuals of the initial estimate. In matrix notation and rearranging terms, noting that $F_i(RA_L, D_L) = 0$,

$$\begin{bmatrix} \rho_1 \\ \rho_2 \\ \cdot \\ \cdot \\ \cdot \\ \rho_n \end{bmatrix} = \begin{bmatrix} \partial F_i/\partial RA_L^\circ & \partial F_1/\partial D_L^\circ \\ \partial F_2/\partial RA_L^\circ & \partial F_2/\partial D_L^\circ \\ \cdot & \cdot \\ \cdot & \cdot \\ \cdot & \cdot \\ \partial F_n/\partial RA_L^\circ & \partial F_n/\partial D_L^\circ \end{bmatrix} \begin{bmatrix} \Delta RA_L \\ \Delta D_L \end{bmatrix} \equiv R \doteq P\Delta.$$

$(n \times 1)$ $(n \times 2)$ (2×1)

If an n-by-n diagonal weighting matrix K^{-1} can be constructed from known error magnitudes in the sensor's cone angle measurements, such that the relative accuracies of each measurement can be reflected in the solution, then

$$\underbrace{K^{-1} R}_{(n \times 1)} = \underbrace{K^{-1} P\Delta}_{(n \times 1)}$$

Specifically,

$$K \equiv \begin{bmatrix} k_1 & 0 & \cdot & \cdot & \cdot & 0 \\ 0 & k_2 & \cdot & \cdot & \cdot & 0 \\ \cdot & \cdot & \cdot & & & \cdot \\ \cdot & \cdot & & \cdot & & \cdot \\ \cdot & \cdot & & & \cdot & \cdot \\ 0 & 0 & \cdot & \cdot & \cdot & k_n \end{bmatrix} \equiv \begin{bmatrix} \sigma^2(\cos\theta_1) & 0 & \cdot & \cdot & \cdot & 0 \\ 0 & \sigma^2(\cos\theta_2) & \cdot & \cdot & \cdot & 0 \\ \cdot & \cdot & \cdot & & & \cdot \\ \cdot & \cdot & & \cdot & & \cdot \\ \cdot & \cdot & & & \cdot & \cdot \\ 0 & 0 & \cdot & \cdot & \cdot & \sigma^2(\cos\theta_n) \end{bmatrix}$$

where $\sigma^2(\cos\theta_i) = +\sin^2\theta_i \sigma^2_{\theta_i}$ in analogy with $\Delta(\cos\theta) = -\sin\theta\ \Delta(\theta)$.

The solution for Δ now follows the usual matrix least squares procedure. First, premultiply both sides of the equation by P^T.

$$\underbrace{P^T K^{-1} R}_{(2 \times 1)} = \underbrace{P^T K^{-1} P}_{(2 \times 2)} \underbrace{\Delta}_{(2 \times 1)} .$$

If the inverse of $(P^T K^{-1} P)$ is nonsingular,

$$(P^T K^{-1} P)^{-1} P^T K^{-1} R = (P^T K^{-1} P)^{-1} (P^T K^{-1} P) \Delta = \Delta,$$

which is the initial correction matrix with elements ΔRA_L°, ΔD_L°. The correction elements are combined with the initial estimates RA_L°, D_L° to form the next estimates in the iteration process. Before returning to the Taylor's expansion, ΔRA_L° and ΔD_L° are compared with the preselected bounds ϵ_1 and ϵ_2. If

$$\Delta RA_L^\circ < \epsilon_1 \textit{ and } \Delta D_L^\circ < \epsilon_2 ,$$

then the solution of the spin axis orientation is accepted as

$$RA_L^\circ + \Delta RA_L^\circ \textit{ and } D_L^\circ + \Delta D_L^\circ .$$

If, as is usual, one or both of the bounds is exceeded, the algorithm repeats.

The inverse of the normal equations $(P^T K^{-1} P)^{-1}$ for each iteration provides another desirable set of solutions; that is, $(P^T K^{-1} P)^{-1}$ is the 2-by-2 variance-covariance matrix of error in the solution correction values.

$$(P^T K^{-1} P)^{-1} = \begin{bmatrix} \sigma^2 RA_L & \sigma RA_L \sigma D_L \\ \sigma RA_L \sigma D_L & \sigma D_L^{\,2} \end{bmatrix}$$

The matrix is formed at each iteration, and when the correction values are found to be acceptable, the standard deviations σRA_L and σD_L are available.

Table 1
Conversion of Digital Solar Attitude Detector
Gray Codes to Sun Angle*

Code Bit No. 7654321	Angle X (deg)	Code Bit No. 7654321	Angle X (deg)	Code Bit No. 7654321	Angle X (deg)
1110101 =	0.5	1110100 =	1.5	1111100 =	2.5
1111101 =	3.5	1111111 =	4.5	1111110 =	5.5
1111010 =	6.5	1111011 =	7.5	1111001 =	8.5
1111000 =	9.5	1101000 =	10.5	1101001 =	11.5
1101011 =	12.5	1101010 =	13.5	1101110 =	14.5
1101111 =	15.5	1101101 =	16.5	1101100 =	17.5
1100100 =	18.5	1100101 =	19.5	1100111 =	20.5
1100110 =	21.5	1100010 =	22.5	1100011 =	23.5
1100001 =	24.5	1100000 =	25.5	0100000 =	26.5
0100001 =	27.5	0100011 =	28.5	0100010 =	29.5
0100110 =	30.5	0100111 =	31.5	0100101 =	32.5
0100100 =	33.5	0101100 =	34.5	0101101 =	35.5
0101111 =	36.5	0101110 =	37.5	0101010 =	38.5
0101011 =	39.5	0101001 =	40.5	0101000 =	41.5
0111000 =	42.5	0111001 =	43.5	0111011 =	44.5
0111010 =	45.5	0111110 =	46.5	0111111 =	47.5
0111101 =	48.5	0111100 =	49.5	0110100 =	50.5
0110101 =	51.5	0110111 =	52.5	0110110 =	53.5
0110010 =	54.5	0110011 =	55.5	0110001 =	56.5
0110000 =	57.5	0010000 =	58.5	0010001 =	59.5
0010011 =	60.5	0010010 =	61.5	0010110 =	62.5
0010111 =	63.5	0010101 =	64.5	0010100 =	65.5
0011100 =	66.5	0011101 =	67.5	0011111 =	68.5
0011110 =	69.5	0011010 =	70.5	0011011 =	71.5
0011001 =	72.5	0011000 =	73.5	0001000 =	74.5
0001001 =	75.5	0001011 =	76.5	0001010 =	77.5
0001110 =	78.5	0001111 =	79.5	0001101 =	80.5
0001100 =	81.5	0000100 =	82.5	0000101 =	83.5
0000111 =	84.5	0000110 =	85.5	0000010 =	86.5
0000011 =	87.5	0000001 =	88.5	0000000 =	89.5

*If bit 8 (not listed above) is a 1-bit, the sun angle = angle X.
If bit 8 is a 0-bit, sun angle = 180° - angle X.

Bit outputs other than those shown result in a flag in the angle value.

where H_x, H_y, and H_z are the measured components.

The field components are read out in analog form in millivolt units from -250 to +250 millivolts, which correspond to physical units of -27.853 to +27.853 amperes/meter (-350 to +350 millioersteds). For telemetry back to earth, the millivolt readings are digitized as 8-bit words. But 8 bits can represent just 256 readings, so that digitization introduces a ±1 millivolt error in each measurement. The formula for converting from digital counts back to millivolts is as follows:

$$\text{If counts} \leqslant 127, \quad \text{millivolts} = 2 \times (\text{counts} - 127).$$

$$\text{If counts} > 127, \quad \text{millivolts} = 2 \times (\text{counts} - 128).$$

This shows that two different counts for zero millivolts is possible—127 or 128.

The final conversion from millivolts to millioersteds is straightforward, since the two values are proportional. Thus

$$\text{Millioersteds} = (\text{millivolts} + 250) \times \frac{700}{500} - 350$$

where (millivolts + 250) = converted millivolts minus lower millivolt limit,

700/500 = the ratio of the range in millioersteds to the range in millivolts, and

-350 = the addition of the lower millioersted limit.

This formula is a linear interpolation technique.

Besides the digitization error of ±1 millioersted, a small error in the magnitude of the magnetic field is introduced by the sampling of the three magnetometers over three consecutive half frames of 0.768 second once each major frame of 49.152 seconds, rather than at the same time. The total effect of all magnetometer measurement errors is estimated to be ±280 milliamperes/meter (±3.5 millioersteds) for the system under operating conditions.*

A chargeable, trim-magnet system, of three chargeable magnets parallel to the spacecraft axes, is included to provide a means of compensating for residual dipole fields from the z-coil if demagnetization is not fully effective. These three trim readouts are in analog voltages corresponding to pole-cm units. The pole-cm units are, in turn, proportional to millioersted units, and are then applied as residual bias corrections to the respective magnetometer values.

Additional analyses of magnetometer data were performed to determine and eliminate other types of systematic error in the magnetic field/magnetometer cone intersection angles. The error sources may have resulted from launch effects or other post-launch conditions, hence

*Meyers, G. F., et al., *SAS-1 Attitude Data Analyses*, GSFC X-542-71-363, 1971.

the systematic errors had to be traced from in-flight information. The principal possible sources of systematic errors were sensor mounting misalignments, magnetometer nonorthogonality, and inate sensor biases. Two different kinds of mounting misalignment were considered: (1) If the spacecraft geometrical symmetry axis and spin axis produced by the spin rotor do not coincide, but are some small angle apart, then the magnetometer triad is misaligned to the spin axis, even when the triad is mounted correctly to the symmetry axis. (2) If the symmetry and spin axes coincide, but the tri-axis magnetometer is mounted with the magnetometers not parallel to their respective spacecraft axes, then the triad is misaligned to the spin axis.

If the individual magnetometers are mounted improperly with respect to each other, such that they are not mutually perpendicular, then systematic errors due to nonorthogonality arise. Finally, if after the chargeable trim magnets and demagnetization of residual coil fields are considered, and magnetic field components do not match the spacecraft magnetometer measurements within a random range, then a remnant, residual spacecraft magnetism and sensor bias is present. Such a residual bias can be present separately for each magnetometer.

The chief difficulty in determining each of the above factors is that they are interdependent. As such, for instance, a misalignment error can easily be interpreted as a contribution to the residual bias. Cross-check and multiparameter programs were developed to circumvent the interdependence problem. The best determination of each of the factors is given in tables 2, 3, and 4. Note that the misalignment factors are not separated according to the two kinds of spin axis-to-magnetometer misalignment. A further study of short term drift, caused by either kind of coning of the tri-axis magnetometer about the spin axis, indicated a possible coning amplitude of about 0.°6 with a period of the order of a spin period. However, the two kinds of misalignment produced the same effects in simulated data, and noise effectively obscured any oscillation attributable to a specific misalignment.

In case of telemetry error or other kind of data loss from one of the magnetometer components, the magnetic field cone angle μ can still be determined from the remaining components, and the geomagnetic field magnitude can be taken from special orbit data tapes or computed from a programmed magnetic field model. If H is the magnetic field magnitude in milligauss and M_x, M_y, and M_z are the field components derived from the magnetometer measurements, then cone angle μ is given by either of the following equations:

$$\cos \mu = \frac{\sqrt{H^2 - M_x^2 - M_y^2}}{H} \qquad \text{for } M_z \text{ not known.}$$

$$\cos \mu = \frac{M_z}{H} \qquad \text{for } M_x \text{ and/or } M_y \text{ not known.}$$

Table 2
Angles Between Magnetometers

Between	Angle (Degrees)
x and y*	90.775 ± 0.090
x and z	90.19 ± 0.38
y and z	89.55 ± 0.47

*Angle not corrected for 0.°37 rotation of spacecraft between x and y readings.

Table 3
Alignment of Magnetometer to Spin Axis

Magnetometer	Angle from Magnetometer to Spin Axis (Degrees)
x	90.06 ± 0.41
y	89.75 ± 0.49
z	0.307 ± 0.088

Table 4
Magnetometer Residual Biases

Magnetometer	Bias	
	Milligauss	Nanotesla
x	-0.23 ± 0.57	- 23 ± 57
y	3.21 ± 0.30	321 ± 30
z	6.23 ± 0.94	623 ± 94

If all components are known, the relation is

$$\cos \mu = \frac{M_z}{\sqrt{M_x^2 + M_y^2 + M_z^2}}$$

The Closed Form Least Squares Method

Another least squares treatment of the spin-axis orientation problem, but one which does not require iterations with small corrections to an estimated solution, is the closed-form least squares (CFLS) method. From the initial set of cone angle equations, one pass through the solution algorithm derives the results. However, an exception to the one-pass condition exists if some of the cone angle data is bad enough to be discarded, and the algorithm is repeated with the reduced data set. Various acceptance criteria could be selected to designate bad data, but the most common is to choose a specific number of standard deviations from the solution parameters as the acceptance limit.

The solution components are the spin-axis inertial Cartesian coordinates, X_s, Y_s, and Z_s, which are involved through the dot-product/ cosine-of-the-cone-angle relation

$$\cos\theta_i = \hat{U}_i \cdot \hat{S} = U_{X_i} X_s + U_{Y_i} Y_s + U_{Z_i} Z_s \quad (i = 1, 2, \ldots, n)$$

where θ_i is the cone angle between the *ith* physical, unit vector $\hat{U}_i$ and the spin axis $\hat{S}$. The n equations of this form can be expressed in matrix notation as

$$\underset{(n \times 1)}{\begin{bmatrix} \cos\theta_1 \\ \cos\theta_2 \\ \cdot \\ \cdot \\ \cdot \\ \cos\theta_n \end{bmatrix}} = \underset{(n \times 3)}{\begin{bmatrix} U_{X_1} & U_{Y_1} & U_{Z_1} \\ U_{X_2} & U_{Y_2} & U_{Z_2} \\ \cdot & \cdot & \cdot \\ \cdot & \cdot & \cdot \\ \cdot & \cdot & \cdot \\ U_{X_n} & U_{Y_n} & U_{Z_n} \end{bmatrix}} \underset{(3 \times 1)}{\begin{bmatrix} X_s \\ Y_s \\ Z_s \end{bmatrix}}$$

which, for convenience, is represented by

$$C = U S \qquad \text{(condition equations).}$$

Using the matrix least squares techniques of Appendix D, premultiply by the transpose of U

$$\underbrace{U^T C}_{(3 \times 1)} = \underbrace{U^T U}_{(3 \times 3)} \underbrace{S}_{(3 \times 1)} \qquad \text{(normal equations)}$$

where $U^T U$ is a 3-by-3 square matrix. If $U^T U$ is nonsingular, then it has an inverse and

$$[U^T U]^{-1} U^T C = S$$

where the elements of S are the components X_s, Y_s, and Z_s. If required, the spherical coordinates are derived as in the section, "Spin-stabilized Spacecraft Attitude," and are illustrated in figure 11.

The addition of a weighting matrix is desirable if *a priori* relative sensor precision is unknown. But, the superiority of one sensor over another is reflected in the standard deviations, σ_i, of each $\cos\theta_i$ measurement. The weighting matrix K^{-1} is therefore given by the inverse of the diagonal variance matrix K of the measurements, where σ_i^2 = variance and $\sin\theta_i \sigma_{\theta_i} = \sigma_i$.

$$K = \begin{bmatrix} \sigma_1^2 & 0 & \cdot & \cdot & \cdot & 0 \\ 0 & \sigma_2^2 & \cdot & \cdot & \cdot & 0 \\ \cdot & \cdot & \cdot & & & \cdot \\ \cdot & \cdot & & \cdot & & \cdot \\ \cdot & \cdot & & & \cdot & \cdot \\ 0 & 0 & \cdot & \cdot & \cdot & \sigma_n^2 \end{bmatrix}$$

The initial equations then take on the form

$$K^{-1} C = K^{-1} U S \qquad \text{(weighted conditional equations),}$$

$$U^T K^{-1} C = [U^T K^{-1} U] S \qquad \text{(weighted normal equations).}$$

The 3-by-3 inverse of $[U^T K^{-1} U]$ in the normal equations is the variance-covariance error matrix for the solution components from which the standard deviations σ_X, σ_Y, and σ_Z are produced.

$$[U^T K^{-1} U]^{-1} = \begin{bmatrix} \sigma_X^2 & \sigma_X\sigma_Y & \sigma_X\sigma_Z \\ \sigma_Y\sigma_X & \sigma_Y^2 & \sigma_Y\sigma_Z \\ \sigma_Z\sigma_X & \sigma_Z\sigma_Y & \sigma_Z^2 \end{bmatrix}$$

Closed Form Least Squares Solution Applied to IMP-6

The IMP-6 spacecraft attitude system and a pair of exact, three-constraint approaches to spin-axis determination have been described above. Application of the CFLS method parallels that of the PQV approach for the computation and selection of the earth nadir/spin axis angle δ. Because the CFLS method is applied to overdetermined sets of data, additional equations such as for the $\hat{V}$ vector or the unit spin axis vector $\hat{S}$ constraint are not required to produce a solution. However, evaluation of the $\hat{V}$ vector components and the angle α between $\hat{V}$ and $\hat{S}$ (as done for the PQV approach) provides a third set of equations which are combined with the others for a better least squares solution. The advantage of adding the V-terms is to constrain the solution in such a way that errors in the P and Q terms cannot combine to bias it in the direction of the V's.

If measured cone angles from the spin axis to the sun and to the earth nadir varied widely between 0° and 180°, constructed vector constraints would not be necessary; but, over the period of time for which the spin axis can be considered stationary, the sun position changes little, and the earth nadir direction and cone angle δ are useful only when the earth is scanned by the earth horizon sensor. Thus, different cone angles in the V-terms serve to improve the least squares solution of S.

The condition equations for the CFLS solution of the cone-intersection attitude problem in general form is therefore

$$\cos\theta_j = U_{X_j} X_s + U_{Y_j} Y_s + U_{Z_j} Z_s \quad (j = 1, 2, \ldots, 3n)$$

where the index j extends to 3n to represent the three specific condition equation subsets:

$$\cos\beta_i = P_{X_i} X_s + P_{Y_i} Y_s + P_{Z_i} Z_s \quad (i = 1, 2, \ldots, n),$$

$$\cos\delta_i = Q_{X_i} X_s + Q_{Y_i} Y_s + Q_{Z_i} Z_s \quad (i = 1, 2, \ldots, n),$$

$$\cos\alpha_i = V_{X_i} X_s + V_{Y_i} Y_s + V_{Z_i} Z_s \quad (i = 1, 2, \ldots, n),$$

where the index i is related to a specific telemetry readout.

ANALYSIS AND EVALUATION

SAS-1 Attitude Solutions

As described above, SAS-1 spin-axis solutions are solved by the cone intersection IDCT approach from magnetometer and sun sensor data. Twenty-eight early orbits of SAS-1 were analyzed by the Attitude Determination and Control Section, GSFC.* These orbits were selected because they occurred before the spacecraft tape recorder stopped functioning. Thus an abundance of good playback data from an entire orbit was available. From these analyses several additional parameters were obtained, such as the orthogonality characteristics of the magnetometer axes, the misalignment of the magnetometer axes to the spacecraft axes, and uncorrected residual magnetic field biases. Nonorthogonality and misalignment adjustments were shown to be slight, but the residual bias corrections improved the solutions appreciably.

For this report, raw data from 11 of the 28 SAS-1 analyzed orbits were acquired and were reduced for solution of the spin axis by the CFLS method. No bias corrections were applied, so that comparison is made with the uncorrected, zero bias IDCT results. Also, 14 orbits of SAS-2 were selected for which star sensor and IDCT solutions exist, but the best evaluations of bias corrections were applied before making the CFLS solutions.

Star Sensor

The Attitude Determination and Control Section produced star sensor solutions in a real-time, operational environment necessitating fast evaluations of the data. While the precision

*Meyers, G. F. et al., *SAS-1 Attitude Data Analyses*, GSFC X-542-71-363, 1971.

of the instruments to one arc-minute indicates accurate solutions, a comparison with definitive star sensor solutions for a few orbits was made to detect any unsuspected variations in the accuracy. This comparison showed the operational solutions to be within a few hundredths of a degree of the definitive star sensor solutions (table 5). This accuracy is sufficient for operational star-sensor spin-axis solutions, to serve as a base for determining the accuracy of a cone intersection solution by the IDCT or CFLS methods.

Table 5
Comparison of Operational with Definitive Star Sensor Solutions

Orbit Number	Operational Spin Axis		Average* Definitive Spin Axis		Arc Difference
	Right Ascension	Declination	Right Ascension	Declination	
386	270°.423	-25°.256	270°.340	-25°.314	0°.100
416	273°.697	-16°.336	273°.674	-16°.458	0°.123
476	279°.792	- 1°.280	279°.674	- 1°.333	0°.052
491	281°.829	- 1°.102	281°.836	- 1°.100	0°.003
523	312°.310	5°.891	312°.359	5°.709	0°.189
537	306°.664	6°.615	306°.643	6°.580	0°.034
584	336°.390	-12°.590	336°.307	-12°.671	0°.115
599	339°.533	-20°.379	339°.472	-20°.470	0°.108

*Average values of right ascension and declination are given.
Deviation in right ascension was between ±0°.059 and ±0°.182.
Deviation in declination was between ±0°.048 and ±0°.158.

Magnetometer-Sun Sensor

To satisfy mission requirements the magnetometer-sun sensor cone angle solutions of the spin axis must be within 5° of the actual, definitive results. To obtain this accuracy by the IDCT, it is necessary to use magnetometer and sun data selected throughout an orbit between changes of the spin-axis orientation. A similar but slightly different procedure is followed for CFLS solutions. Table 6 gives the IDCT and star solutions by orbit for the 28 playback orbits which were analyzed. There are three solutions under IDCT representing the three different residual bias considerations. Specifically, these are (1) the case with no residual magnetic field correction; (2) the case with no bias in the x and y magnetometers and a 239 milliampere/meter (+3 millioersted) bias in the z-magnetometer; and (3) the case with no bias in the x, a +3 millioersted (moe) bias in the y, and a 398 milliampere/meter (+5 millioersted) bias in the z-magnetometer. The no-bias corrections case, (1) above,

Table 6

Comparison of Operational Star Solutions with IDCT Solutions for Different Residual Magnetic Field Biases

Orbit	Star		IDCT with biases x, y, z = (0, 0, 0)		IDCT with biases x, y, z = (0, 0, 3)		IDCT with biases x, y, z = (0, 3, 5)	
	Right Ascension	Declination	Right Ascension	Declination	Right Ascension	Declination	Right Ascension	Declination
370	327°.78	-30°.01	328°.39	-29°.06	328°.37	-29°.53	328°.33	-29°.84
386	270°.75	-25°.25	270°.51	-24°.32	270°.53	-24°.86	270°.56	-25°.23
387	270°.83	-25°.25	270°.87	-24°.42	270°.91	-24°.97	270°.94	-25°.33
416	274°.00	-16°.32	274°.67	-15°.20	274°.40	-15°.80	274°.23	-16°.19
432	268°.05	-12°.78	268°.58	-11°.53	268°.26	-12°.16	268°.06	-12°.58
446	275°.64	-11°.13	276°.19	-10°.22	275°.80	-10°.83	274°.80	-11°.14
447	275°.57	-11°.09	275°.54	-10°.09	275°.09	-10°.72	275°.53	-11°.24
476	280°.06	- 1°.26	281°.33	- 0°.18	280°.45	- 0°.78	279°.91	- 1°.18
477	280°.02	- 1°.32	281°.69	- 0°.04	280°.73	- 0°.67	280°.09	- 1°.11
478	279°.89	- 1°.21	283°.63	- 0°.82	281°.69	- 0°.18	280°.52	- 0°.86
491	282°.10	- 1°.08	284°.80	- 0°.12	283°.76	- 0°.49	283°.06	- 0°.91
502	298°.57	3°.12	299°.50	3°.66	299°.31	3°.22	299°.17	2°.93
506	298°.06	3°.40	296°.81	4°.11	296°.96	3°.70	297°.03	3°.41
523	312°.57	5°.97	310°.44	6°.68	311°.27	6°.17	311°.80	5°.84
537	306°.92	6°.68	304°.36	7°.48	305°.21	7°.01	305°.83	6°.69
538	306°.77	6°.84	304°.30	7°.48	305°.23	7°.03	305°.89	6°.72
539	305°.53	6°.89	304°.74	7°.46	305°.54	7°.04	306°.12	6°.74
552	300°.46	8°.83	299°.56	9°.47	299°.43	9°.06	299°.41	8°.79
553	300°.23	8°.81	299°.59	9°.38	299°.71	9°.03	300°.03	8°.80
554	300°.20	8°.74	299°.89	9°.50	300°.11	9°.12	300°.26	8°.86
577	337°.02	-13°.83	336°.96	-11°.93	337°.17	-12°.56	337°.30	-12°.99
584	336°.67	-12°.48	336°.26	-11°.52	336°.44	-12°.08	336°.54	-12°.46
599	339°.82	-20°.26	339°.75	-19°.21	339°.82	-19°.81	339°.86	-20°.21
605	343°.69	-13°.56	343°.48	-12°.60	343°.67	-13°.21	343°.78	-13°.61
611	338°.17	-13°.92	337°.48	-12°.57	337°.65	-13°.21	337°.75	-13°.64
612	338°.77	-14°.24	337°.71	-12°.64	337°.88	-13°.26	337°.98	-13°.67
613	337°.88	-13°.78	337°.67	-12°.65	337°.82	-13°.23	337°.91	-13°.61
627	337°.96	-13°.76	337°.54	-12°.48	337°.68	-13°.09	337°.78	-13°.49

produces adequate solutions; the (0, 0, 3) millioersted corrections case, (2) above, corresponds to the prelaunch determination and improves the solution; but the in-flight determined (0, 3, 5) case, (3) above, clearly is the best with a mean arc error of 0°.47 compared to 1°.50 and 0°.81, respectively.

Table 7 is the set of CFLS solutions compared with star solutions for 11 of the 28 orbits for which raw telemetry and orbit data were specifically reduced. The distinction between the two different CFLS solution columns is that for the CFLS/PQ case the input equations consisted of the sensor cone angles and the vector components of the sun and magnetic field only, but for the PQV case the normal vector $\vec{V}$ and its associated cone angle were added to the equations. From this table the CFLS/PQV approach is seen to be much stronger. The reason for this is that the CFLS/PQ equations do not produce good geometrical constraints on the solution, since the magnetic field vectors are all within a few degrees of arc and the sun vectors vary by only one degree. This condition magnifies errors and creates the inaccurate CFLS/PQ solutions. The orbits 386, 387, 553, and 554 had data selected from throughout the orbit and, therefore, had a wider range of magnetic field vector positions, which resulted in significantly more accurate solutions. The CFLS/PQV equations provided strong geometrical constraints and resulted in significantly more accurate solutions.

Table 7
Comparison of Operational Star Solutions with CFLS Solutions

Orbit	Star		CFLS/PQ		CFLS/PQV	
	Right Ascension	Declination	Right Ascension	Declination	Right Ascension	Declination
370	327°.78	-30°.01	338°.54	-18°.57	328°.68	-28°.76
386	270.75	-25.25	272.53	-23.09	270.83	-23.25
387	270.83	-25.25	262.96	-23.42	271.30	-22.42
416	274.00	-16.32	280.85	-12.33	275.12	-13.73
432	268.05	-12.78	273.94	-10.38	269.84	-10.78
446	275.64	-11.13	248.00	-14.58	279.36	- 8.02
447	275.57	-11.09	272.36	-10.39	275.80	- 9.85
553	300.23	8.81	299.02	10.20	296.33	9.14
554	300.20	8.74	297.28	9.81	295.24	9.05
577	337.02	-12.83	348.31	-14.46	336.52	-11.71
599	339.82	-20.26	340.29	-13.26	341.43	-19.18

Comparison of SAS-1 IDCT and CFLS Solutions

For direct comparison of the IDCT with the CFLS results, table 8 is given. Qualifying explanations of the CFLS solutions are necessary, however, to interpret the results. From tables 6, 7, and 8, it is apparent that the CFLS solutions are significantly less accurate than even the no-bias IDCT values, but operational conditions account for some of the variation.

Table 8
Comparison of CFLS with IDCT Solutions

Orbit	Star		CFLS/PQV		IDCT (0,0,0) Bias	
	Right Ascension	Declination	Right Ascension	Declination	Right Ascension	Declination
370	327°.78	-30°.01	328°.68	-28°.76	328°.39	-29°.06
386	270.75	-25.25	270.83	-23.25	270.51	-24.32
387	270.83	-25.25	271.30	-22.42	270.87	-24.42
416	274.00	-16.32	275.12	-13.73	274.67	-15.20
432	268.06	-12.78	269.84	-10.78	268.58	-11.53
446	275.64	-11.13	279.36	- 8.02	276.19	-10.22
447	275.57	-11.09	275.80	- 9.85	275.54	-10.09
553	300.23	8.81	296.33	9.14	299.59	9.38
554	300.20	8.74	295.24	9.05	299.89	9.50
577	337.02	-12.83	336.52	-11.71	336.96	-11.93
599	339.82	-20.26	341.43	-19.18	339.75	-19.21

That is–

- For all orbits except 386, 387, 553, and 554, data were selected from a few short time intervals rather than scattered evenly throughout the full orbits. The short time intervals were about 5 minutes in duration and corresponded to periods of properly correlated time between universal time and the spacecraft clock.
- The sun angle readings were accurate only to within 1°; yet, alterations of 0°.1 in tests of orbits 553 and 554 produced deviations of arc from 1° to 2°. Daily records and analysis would allow interpolation of the sun angle to an accuracy of less than 0°.5. (For IMP-6 such interpolation provides sun angle values good to 0°.05.)
- The magnetic field magnitudes computed from telemetry data differed from the field magnitudes supplied by the Orbit Determination and Control Section by up to +1600 to -800 milliamperes/meter (+20 to -10 millioersteds). The field quantities derived from telemetry were used in computing cone angles for consistency and to minimize any systematic error; but as has been shown in the residual bias comparison on the IDCT solutions, a remnant difference of a few millioersteds affects the solutions proportionately.
- Interpolation from telemetry time to the nearest minute was not made on the measured magnetic field components to bring them to the same time as the magnetic field model inertial coordinates, because the measured z-components were not varying significantly in those few seconds; but the x- and y-components, which had to be interpolated, varied to a greater degree than the field model would indicate as likely.

Table 9
CFLS Solution Errors in Right Ascension, Declination, and Arc
and the Standard Deviation in Arc for Each Orbit

Orbit	ΔRight Ascension	ΔDeclination	ΔArc	$\tilde{\sigma}$ Arc
370	+0°.89	+1°.25	1°.47	0°.72
386	+0.08	+2.00	2.01	0.74
387	+0.47	+2.73	2.86	0.71
416	+1.12	+2.59	2.81	0.83
432	+1.78	+2.00	2.66	0.72
446	+3.72	+3.12	4.82	0.94
447	+0.23	+1.24	1.26	0.94
553	-3.90	-0.23	3.87	0.745
554	-4.96	-0.31	4.91	0.70
577	-0.50	+1.12	1.22	0.945
599	+1.61	+1.08	1.86	0.90

Error Analysis

Table 9 is a summary of all of the errors in the CFLS/PQV solutions. Typical errors are given by the differences between the CFLS solutions and the star solutions in right ascension, declination, and arc. These differences are equivalent to the net effect of the errors caused by individual data point contributions. The means of these errors are as follows:

$$\overline{\Delta \text{ RA}} = +0°.02$$

$$\overline{\Delta \text{ Dec}} = +1°.51$$

$$\overline{\Delta \text{ Arc}} = 2°.70$$

Note that the trend of these errors is positive, indicating a systematic error presence consistent with the comparison qualifications described in the section above.

The strongly negative differences for orbits 553 and 554 indicate the possibility of another factor at work in these orbits, and this in fact is the case. Since data for 553 and 554 were selected at several different time intervals throughout the orbit, the solutions for these orbits were expected to be superior. Checking the CFLS/PQ solutions (table 7) shows that the best results for 553 and 554 were obtained by that procedure:

Orbit:	553	554
Right ascension:	-1°.21	-2°.92
Declination:	+1°.39	+0°.77
Arc:	1°.84	3°.00

Examination of the CFLS/PQV equations shows that the geometry for the computation of the V-vector-to-spin-axis cone angle involved the sum of two spherical triangle legs (β and δ), which was less than the third leg (η). This condition existed due to subtractive errors in the measurements of β and δ, combined with the situation of the spin axis becoming aligned with the plane of the sun and the magnetic field vector, making $\beta + \delta \approx \eta$, with large variations in the cosines of small angles for small deviations in the angles. An alternative angle determination scheme can be incorporated in the algorithm to bypass this problem.

The root-mean-square (rms) error can be determined for any data which has a mean, and it is useful for finding the range about an arbitrary origin in which new data is likely to fall. For the situation where the data is taken as the spin-axis difference components between the star solution and the cone angle solution for each orbit, the rms is

$$\sqrt{\sum_i (\Delta_i^2)/N}$$

where Δ_i = one of the difference components ΔRA_i, ΔDec_i, or ΔArc_i, and

N = the number of total orbits.*

These values are

$$RMS_{\Delta RA} = 2.^{\circ}33$$

$$RMS_{\Delta Dec} = 1.^{\circ}85$$

$$RMS_{\Delta Arc} = 2.^{\circ}99$$

and the ΔRA have been normalized to degrees of arc. (See the section on SAS-2 error analysis for further discussion.)

The standard deviations of the angle components for the entire set of orbit solutions takes the form—

$$\sigma_\Delta = \sqrt{\frac{\sum_i (\Delta_i - \bar{\Delta})^2}{N - 1}}$$

where Δ_i is as defined above, $\bar{\Delta}$ is the average of that component over all orbits, and N-1 is is the degree of freedom (one constraint being used in the determination of the mean $\bar{\Delta}$).

*Kirby, P. et al., *Data Processing Plan for Small Astronomy Satellite (SAS-A)*, GSFC X-564-71-130, December 1970.

The properties of the standard deviation are well known, such that the selection of a new orbit data set should produce a solution which differs from the appropriate star solution in right ascension by less than $\sigma_{\Delta RA}$, in declination by less than $\sigma_{\Delta Dec}$, and in arc by less than $\sigma_{\Delta Arc}$, 68 percent of the time in each case. These values are–

$$\sigma_{\Delta Arc} = 1.^{\circ}33$$

$$\sigma_{\Delta RA} = 2.^{\circ}43$$

$$\sigma_{\Delta Dec} = 1.^{\circ}11$$

An indirect computation of the standard deviations of the parameters from a least squares solution can be obtained without resorting to separate spin-axis solutions of each set of sensor measurements. These standard deviations are derived from the inverse of the normal matrix, N^{-1} ($= [U^T U]^{-1}$; see the section above, "The Closed-form Least Squares Method" and Appendix D). This matrix is called the variance-covariance matrix of the solution. The diagonal elements of N^{-1} are extracted, and are the normalized, nondimensional variances of the solution parameters. To obtain the required variances (squares of the standard deviations), a multiplicative factor–the square of the standard error of a single measurement–must be introduced. If $\hat{\sigma}^2_{xx}$, $\hat{\sigma}^2_{yy}$, and $\hat{\sigma}^2_{zz}$ are the diagonal elements, then the true variances are

$$\tilde{\sigma}_{xx}^{\,2} = m^2 \hat{\sigma}_{xx}^{\,2} \; ; \; \tilde{\sigma}_{yy}^{\,2} = m^2 \hat{\sigma}_{yy}^{\,2} \; ; \; \tilde{\sigma}_{zz}^{\,2} = m^2 \hat{\sigma}_{zz}^{\,2} \, .$$

If the variances are desired in spherical rather than Cartesian coordinates, differentiation properties apply such that

$$\hat{\sigma}_{RA} = \frac{\pm (x\sigma_{yy} - y\sigma_{xx})}{x^2 + y^2} \quad \text{and} \quad \hat{\sigma}_{Dec} = \frac{\hat{\sigma}_{zz}}{(1 - z^2)^{1/2}}$$

$$\left[\text{from } \sigma (\tan \alpha) = \sigma (x/y) = \frac{\sigma_\alpha}{\cos^2 \alpha} = \frac{x\sigma_y - y\sigma_x}{x^2} \right.$$

where

$$\cos^2 \alpha = \frac{x^2}{x^2 + y^2}$$

and

$$\sigma (\sin \delta) = \sigma (z) = \cos \delta \, \sigma_z$$

where

$$\left. \cos \delta = \sqrt{1 - z^2} \right] .$$

However, a more useful variance is the net or total arc variance,

$$\hat{\sigma}^2_{Arc} = (\sigma_{xx}{}^2 + \sigma_{yy}{}^2 + \sigma_{zz}{}^2),$$

which, with the appropriate multiplicative factor, gives the distribution of angular error around the spin axis solution. That is, the standard deviation

$$\tilde{\sigma}_{Arc} = m\hat{\sigma}_{Arc}$$

is the radius around the solution of the spin-axis vector for a particular orbit, within which another spin-axis solution, based on similar measurements, would fall 68 percent of the time. A good estimate of m for the determination of $\tilde{\sigma}_{Arc}$ is the average of the magnetometer standard error and the sun sensor standard error—(1°.5 + 0°.5)/2 = 1°—for all sensor readings in each orbit. The results of this assumption are shown in table 9 for $\tilde{\sigma}_{Arc}$.

Peak arc errors of about 5° for orbit 554 and about 4° for 553 were examined above and were attributed to a geometrical configuration of the sun, magnetic field, and spin axis vectors, which, under the present algorithm, tend to propagate errors in this situation rather than damp them out.

The peak arc error of nearly 5° for orbit 446 is clearly related to the CFLS/PQ solution arc error for that orbit of nearly 30°. Obviously, a gross error is present in the data, though a careful check of all values indicates that whatever error is present is due to inaccuracies in the raw data.

Continued analysis and refinement of the CFLS method as applied to SAS, and increased care in the solution and reduction of data, would reduce error peaks to the present mean value, and would tend to produce solution accuracies approaching the IDCT results. Five-degree accuracy is obviously obtained, and operational accuracies of 2° or better are indicated and were achieved for SAS-2 data, as will be explained below.

SAS-2 Attitude Solutions

The SAS-1 CFLS spin-axis solutions in the section, "SAS-1 Attitude Solutions," were based on certain prelaunch determined spacecraft parameters, and were discussed with no consideration of bias or calibration adjustments to the magnetometer data. This approach is reasonably accurate, but incorporation of bias and recalibration values significantly improve the solutions. The results obtained by using such computed adjustments will be considered in this section.

SAS-2 spin axis solutions for certain orbits for which IDCT solutions exist were redetermined using the CFLS method. In addition to the no-bias and nominal calibration solutions, CFLS solutions based on residual spacecraft magnetism and sensor biases and new millivolts-to-millioersted calibration equations (as determined by the Attitude Determination and Control Section) were obtained. Comparison is made here, for each orbit, of the operational star solutions (considered as accurate) with the nominal calibration (discussed in the section,

"IDCT Solution Applied to SAS-1"), the no-bias correction IDCT and CFLS solutions, and with the best bias, recalibrated CFLS solutions.

IDCT solutions with the best bias and recalibration values were not available for the selected orbit data, but another group of orbits for which such IDCT solutions exist provided statistics for comparison with CFLS solution statistics. Nonorthogonality and misalignment adjustments were found to be very small and were ignored.

Bias and Recalibration Parameters

Determination of SAS-2 residual magnetic field bias corrections and millivolts-to-millioersted (milliampere/meter) calibration parameters is made by solving a single equation for each axis. The equation is

$$
\begin{aligned}
f_i V_i = {} & \sin\theta_i \cos(\omega t + \phi_{0_i})(H_X \sin\delta \cos\alpha + H_Y \sin\delta \sin\alpha - H_Z \cos\delta) \\
& + \sin\theta_i \sin(\omega t + \phi_{0_i})(-H_X \sin\alpha + H_Y \cos\alpha) \\
& + \cos\theta_i (H_X \cos\delta \cos\alpha + H_Y \cos\delta \sin\alpha + H_Z \sin\delta) + B_i
\end{aligned}
$$

where H_X, H_Y, and H_Z = the inertial components of the earth's magnetic field, determined at the spacecraft position from a theoretical model of the earth's magnetic field;

V_i = the voltage in millivolts from a particular magnetometer axis ($i = x, y, z$);

α and δ = the right ascension and declination components, respectively, of the spin axis;

ω = the spin rate;

θ_i = the alignment angle of the *ith* magnetometer axis;

ϕ_{0_i} = the initial ($t = 0$) azimuth of the *ith* magnetometer axis;

f_i = the slope of the *ith* magnetometer axis calibration curve (in moe/mv), and

B_i = the *ith* magnetometer axis bias (in moe).

The form of this equation results from transforming the inertial coordinates of the magnetic field model vector into the spacecraft reference frame (spin axis = z axis), and projecting these components onto each of the magnetometer axes. (See figures 18 and 19.) This is equivalent to taking the dot product between the magnetic field vector in spacecraft coordinates and the magnetometer axis unit vector. The B term is the linear addition of the residual bias.

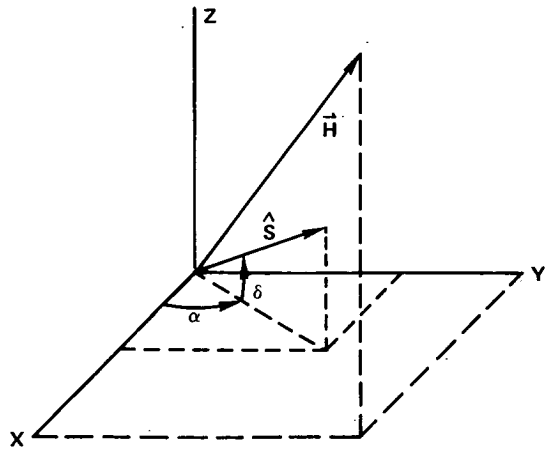

Figure 18. Magnetic Field Vector H and Spin Axis in Ŝ in Inertial Coordinates

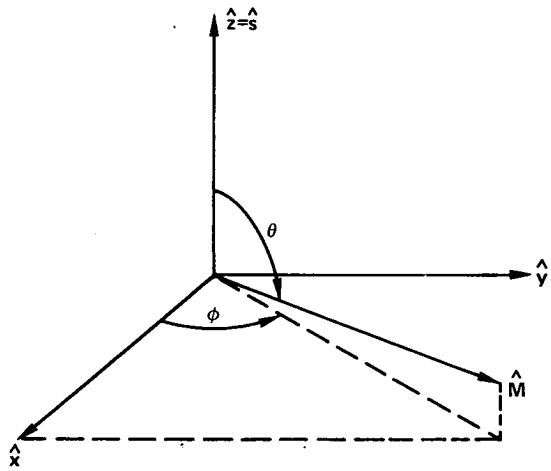

Figure 19. Magnetometer Axis M̂ in Spacecraft Coordinates

The equation can be solved in a least squares sense for any of the last seven parameters, since over a given time interval within an orbit they are nearly constant and the equation can be overdetermined.

For final determination of f_i and B_i (i = x, y, z), selection of the best values for the other parameters from prior solutions and other methods is made, and an iterative, differential correction least squares fit is performed on the equations with the other parameters held constant. Results were taken over many orbits and averaged to the nearest millioersted for B_i and to the moe/mv ratio of whole numbers nearest the nominal ratio of 700/500 for f_i.

The initial determinations were for the biases only—not including the recalibration slopes—and produced the residual magnetic field biases of x = 0, y = 0, and z = -7. While the magnitudes of the magnetic field computed using these biases were better than fields computed using the (0, 0, 0) bias set, when compared with the field model values, the spin axis solutions derived from the (0, 0, -7) set were not as close to operational star solutions as were solutions based on the (0, 0, 0) set. This was interpreted as a requirement for computation of the calibration slopes. The resultant recalibrated millivolts-to-millioersted conversion equation for the x- and y-axes was

$$\text{millioersted} = (\text{millivolts} + 254)(728/508) - 364$$

and for the z-axis was

$$\text{millioersted} = (\text{millivolts} + 254)(764/508) - 382.$$

The residual bias corrections were x = -1, y = +1, and z = +2. This set of bias corrections and calibration slopes led to more accurate attitude solutions relative to the star solutions and to magnetic field magnitudes closest to the field model.

The presence of bias adjustment values, however, does not necessarily indicate an actual residual magnetism on the spacecraft, but could mean that the millivolts-to-millioersted conversion calibration is offset such that a zero millivolt reading actually reflects a nonzero field value.

Comparison of SAS-2 Attitude Solutions by Various Methods

Operational star, IDCT, and CFLS solutions are given in table 10 for 13 orbits. The IDCT solutions are based on the nominal calibration (slope of curve = 700/500) and no residual bias computation of the magnetic field from the magnetometer readings. The CFLS solutions are based on both the nominal calibration (no-bias computation and a nominal calibration, z-axis bias of -7) and a recalibrated (biased by -1, 1, 2) field computation, and are listed separately. The CFLS solutions are all arrived at by the CFLS/PQV approach discussed in the section on the magnetometer-sun sensor.

The arc differences show a clear improvement in solutions derived from the recalibrated, biased CFLS approach over the nominal calibration cases. Solutions with the (0, 0, -7) bias are less accurate for nearly every orbit, yet the magnetic field vector magnitudes computed with this bias are closer to the field model vector magnitudes than the magnitudes of the (0, 0, 0) biased vectors. The average magnitude differences over each orbit between magnetometer-measured field vectors and the corresponding field-model vectors are given in table 11.

Table 11 reflects the area of improvement of solutions when a jointly derived bias set and recalibration are included in determination of magnetometer-measured fields. A slight reduction of the -1, +1, +2 biases causes the "magnetometer-model" differences to be more positive, hence closer to zero, and the magnetometer-derived magnetic field magnitudes would be closer to the model values. Improvement of the spin axis solutions, however, is not assured—compare the (0, 0, 0) and (0, 0, -7) results—and field magnitude differences over the entire range of 2000 orbits for which the bias/recalibration determination was made should show both positive and negative values, and the average should tend to zero. Other parameters possibly contributing to attitude solution errors are considered more fully in the next section.

For comparison with the recalibrated, bias-derived CFLS solutions, a separate set of orbits solved using the recalibrated, bias-derived IDCT is necessary, since such solutions for the

Table 10
Comparison of Operational Star Solutions with IDCT and CFLS Solutions

	Star		IDCT Bias = (0,0,0); Slope=700/500			$CFLS_1$ Bias = (0,0,0); Slope=700/500			$CFLS_2$ Bias = (0,0,-7); Slope=700/500			$CFLS_3$ Bias = (-1,1,2); Slopes = {728/508 X & Y; 764/508 Z}		
Orbit	RA	Dec	RA	Dec	Arc |☆-IDCT|	RA	Dec	Arc |☆-$CFLS_1$|	RA	Dec	Arc |☆-$CFLS_2$|	RA	Dec	Arc |☆-$CFLS_3$|
1063	262°48	-26°29	262°68	-26°01	0°33	262°68	-25°92	0°41	262°80	-27°38	1°12	262°77	-26°23	0°27
1068	266.23	-27.29	266.46	-27.80	0.55	266.48	-26.79	0.56	266.69	-28.26	1.05	266.57	-27.21	0.32
1072	267.04	-27.37	266.80	-26.86	0.56	266.77	-26.70	0.71	266.85	-28.06	0.72	266.85	-27.45	0.18
1083	264.53	-27.36	264.23	-27.07	0.40	264.25	-26.79	0.63	264.32	-28.24	0.89	264.32	-27.18	0.26
1088	265.21	-27.59	265.74	-26.99	0.76	265.74	-26.95	0.79	265.79	-28.35	0.92	265.82	-27.59	0.54
1093	265.92	-27.86	266.10	-27.54	0.36	266.09	-27.64	0.26	266.19	-29.07	1.23	266.20	-27.99	0.28
1098	266.75	-28.16	266.52	-27.89	0.34	266.56	-27.50	0.68	266.69	-28.91	0.75	266.65	-28.06	0.14
1103/1104	264.61	-27.69	263.84	-27.20	0.84	263.70	-26.88	1.15	263.57	-28.45	1.21	263.60	-27.70	0.90
1108	265.20	-28.07	265.01	-27.78	0.33	265.02	-27.83	0.29	265.16	-28.97	0.90	265.11	-28.33	0.27
1113	266.40	-28.60	266.42	-28.27	0.33	266.56	-27.94	0.67	266.68	-29.36	0.80	266.64	-28.43	0.27
1118	263.78	-28.04	263.54	-27.40	0.68	263.49	-27.32	0.77	263.52	-28.72	0.72	263.56	-28.02	0.20
1124	264.80	-28.49	265.12	-28.18	0.41	265.05	-28.23	0.33	265.16	-29.51	1.07	265.15	-28.56	0.31
1128	266.12	-28.87	265.40	-28.51	0.73	265.41	-28.24	0.89	265.53	-29.71	0.99	265.48	-28.75	0.58

Table 11
Comparison of Magnitudes of Magnetic Field Model Vectors
with Magnetometer-derived Field Vectors

Orbit	Averages of Differences Between Magnetometer-derived and Field Model Magnitudes					
	(0, 0, 0) Bias Nominal Calibration		(0, 0, -7) Bias Nominal Calibration		(-1, +1, +2) Bias Recalibration	
	moe*	mA/m	moe	mA/m	moe	mA/m
1063	-7.68	-611.15	-5.67	-451.20	-0.37	- 15.31
1068	-7.77	-618.32	-4.98	-396.29	-0.52	- 41.38
1072	-9.39	-747.23	-6.01	-315.13	-0.59	- 46.95
1083	-8.77	-697.89	-6.33	-503.72	-1.08	- 85.94
1088	-8.75	-696.30	-5.56	-442.45	-0.04	- 3.18
1093	-8.89	-707.44	-6.31	-502.13	-0.84	- 66.84
1198	-9.15	-728.13	-6.25	-497.36	-1.54	-122.55
1103/1104	-9.27	-737.68	-6.00	-477.46	-0.83	- 66.05
1108	-9.21	-732.91	-5.65	-449.61	-0.57	- 45.36
1113	-8.01	-637.41	-5.35	-425.74	-0.55	- 43.77
1118	-9.27	-737.68	-6.00	-477.46	-0.69	- 54.91
1124	-9.14	-727.34	-6.57	-522.82	-1.39	-110.61
1128	-7.80	-620.70	-5.10	-405.84	-0.75	- 59.68

*Millioersteds

orbits of table 10 were not determined. Table 12 reproduces these results, and an analysis of them with respect to the data of table 10 is provided in the following section.

Error Analysis

Deviations of the magnetometer/sun sensor spin-axis solutions from the operational star-sensor solutions are expected because of uncertainties and errors in the sensor measurements. Random errors tend to cancel when many measurements are used, and systematic errors lessen as the uncertainties in the measurements are resolved. Improvement of solutions due to recalibration and biasing of the magnetometers has been noted above.

Table 12
Recalibration and Bias-derived IDCT Solutions

Method/ Component	Orbit Number								
	599	775	987	1148	1340	1422	1659	1685	1796
☆ Right Ascension	66°05	244°52	186°55	264°69	19°57	139°34	288°26	320°07	7°47
☆ Declination	4.57	- 15.33	14.17	- 28.31	-71.55	- 47.12	24.93	49.13	62.04
IDCT Right Ascension	66.4	244.48	186.51	264.69	19.31	138.82	288.61	320.36	7.95
IDCT Declination	4.6	- 15.72	14.24	- 28.49	-71.92	- 47.63	25.11	49.39	62.14
Arc |☆-IDCT|	0.35	0.39	0.08	0.18	0.38	0.62	0.36	0.32	0.25
Δ Right Ascension	0.35	0.04	0.04	0.0	0.26	0.52	0.35	0.29	0.48
Δ Declination	0.03	0.39	0.07	0.18	0.37	0.51	0.18	0.26	0.10

Further improvement of solutions is expected if sun angle values are refined. This refinement is possible by reducing the systematic error in the sun angle measurements created by the ±0°.5 resolution limitation of the sun sensor. That is, a time history of the sun angle measurements and interpolation between the sun angle changes can produce values good to 0°.1.

With the sensor measurements corrected or specified to the precision limits of the sensor, a residue systematic error and any net random error remain. Table 13 presents an error summary of solutions by the various methods given in the previous section, compared with operational star solutions. All of the measures of dispersion indicated in table 13 relate to the components of the solution differences in such a way as to point up systematic errors, inaccuracies, and imprecisions in the measurements involved in the solutions.

The averages are the arithmetic means of the differences between the sun sensor-magnetometer and star sensor solution components (right ascension, declination, and arc separation), and indicate the accuracy of the set of cone angle solutions with respect to the set of star solutions. Large (>0°.5) dispersions in the right ascension and declination components also reflect a probable systematic error.

The rms deviations are measures of dispersion of the weighted magnitudes of the differences and indicate the range about the star solution component within which an arbitrary cone-angle-solution component is most probable. This is another estimator of the accuracy of the cone-angle solutions.

The standard deviations are measures of dispersion of the solution differences about the mean of the differences, and thus serve as an indicator of the precision of the solutions. If the average component difference is zero, then the σ and rms entries coincide except for a $\sqrt{N/(N-1)}$ term which must be factored from σ (where N is the number of solutions, $N = 13 \therefore \sqrt{N/(N-1)} = \sqrt{13/12} = 1.04$).

The arc separation and declination differences are consistent statistics for any solutions, in that a degree of arc or declination is the same regardless of coordinates. A degree of right ascension, however, varies in size in proportion to the declination. To cancel this effect, right ascension error statistics have been normalized and are expressed in degrees of arc for valid comparison.

The ΔRA averages are close to zero for all methods, with the ΔRA's rms and σ entries accordingly almost coinciding. However, the rms and σ magnitudes from the CFLS methods are around 0°.4, signifying a large range in ΔRA values.

The ΔDec averages show considerable variation, with the recalibrated, biased CFLS solution average being significantly smaller than the others. In addition, the rms and σ entries for that method are small, and show high accuracy and precision due to proper data adjustment.

The large differences between the rms and σ values for the other CFLS methods, with σ being much better than rms, reflect the systematic errors present in the improperly or

Table 13
Statistical Comparison of the Accuracies of IDCT and CFLS Solutions with Respect to Operational Star Solutions

Method/ Bias/ Calibration	Statistics								
	Right Ascension Differences			Declination Differences			Arc-derived Values		
	$\overline{\Delta RA}$*	RMS Dev. of ΔRA	$\sigma_{\Delta RA}$	$\overline{\Delta Dec}$	RMS Dev. of ΔDec	$\sigma_{\Delta RA}$	$\overline{Arc}$	RMS Dev. of Arc	$\sigma_{\Delta Arc}$
IDCT/ (0, 0, 0)/ Nominal	0°.08	0°.34	0°.36	-0°.33	0°.42	0°.29	0°.51	0°.54	0°.19
CFLS/ (0, 0, 0)/ Nominal	-0.09	0.37	0.38	-0.53	0..57	0.21	0.63	0.67	0.27
CFLS/ (0, 0, -7)/ Nominal	0.01	0.39	0.42	0.87	0.88	0.17	0.95	0.97	0.18
CFLS/ (-1, +1, +2)/ Recalibrated	0.03	0.38	0.41	-0.01	0.12	0.13	0.35	0.40	0.22
IDCT/ (-1, +1, +2)/ **Recalibrated	-0.06	0.22	0.22	0.09	0.28	0.28	0.33	0.36	0.15

* $\overline{\Delta RA}$ = Averages of the differences in right ascension between the star and the magnetometer-sun sensor solutions.
RMS Dev. of ΔRA = Root-mean-square deviations in the right ascension differences.
$\sigma_{\Delta RA}$ = Standard deviations of the right ascension differences about the mean of the differences.
** Based on the separate set of orbits of table 12.

unadjusted approaches. The IDCT declination statistics are good, but seem significantly less accurate and precise.

The arc statistics, on the other hand, suggest that the IDCT method gives slightly better solutions than the best CFLS approach, but the average arc deviation and a ±1 standard-deviation range around the average for each method shows the IDCT range to be encompassed by the range from the biased, recalibrated CFLS solutions. Any preference of method, then, seems to be unwarranted, based on these statistics from nonidentical orbits.

A few additional statements should be made to further interpret or clarify the statistics.

- An error in the sun angle has its strongest effect on the right ascension of these spin axis solutions, due to the constraint that the sun's declination is always within ±23°.5, and to the fact that the spin axis declination is approximately -27°. Thus, an inaccuracy in the sun angle expands or contracts the circle of possible solution points, which in the neighborhood of these solutions is primarily a change in right ascension.

  Similarly, the direction of a magnetic field vector detected from the SAS-2 orbit is constrained between +60° and +80° declination, which causes any magnetic field error to show up primarily as an error in the calculated spin-axis declination.

  From these conditions, it is apparent why the solution statistics improved so significantly in the declination but not in the right ascension of the biased, recalibrated CFLS solutions. The significantly better values in the right ascension statistics for the IDCT method possibly can be attributed to two factors: (1) Different sun position-spin axis relationships lessen the right ascension sensitivity to sun angle error in the IDCT data. (2) Sun angle interpolation may have been employed on the IDCT data to give better than ±0°.5 accuracy. This was not done with the CFLS reduced data.

- The arc is a magnitude measurement with only positive contributions to arc statistics; thus no cancellation of positive and negative elements is possible. This means that random effects cannot cancel out, but must be a part of the final net averages. Similarly, the right ascension and declination rms and σ statistics have no cancellations (since terms are squared), and so include all random error components.

- The magnetometer and sun sensor data were selected independently of the star sensor data for each orbit; therefore solutions based on perfect magnetometer-sun sensor readings and calibrations would not be identical to star sensor solutions. This is because of the slow drift of the spin axis vector over an orbital period, and the resultant, slightly-differing solutions based on data taken at different times.

- The standard deviations of the spin-axis spherical coordinates of each orbit were computed directly from a series of biased, recalibrated PQV solutions for each set of sensor measurements related to the CFLS (-1, 1, 2) solution, in contrast to the variance-covariance matrix approach of the section on SAS-1 error analysis. These

statistics are presented in table 14. Note the small variations in $\tilde{\sigma}_{RA}$. This is a result of the strong dependence of the RA solution components on the sun sensor measurements, and since the sun sensor showed no change over a single 95-minute orbit, a high precision in this component is expected.

The $\tilde{\sigma}_{Arc}$ and $\tilde{\sigma}_{Dec}$ elements accordingly almost coincide. These statistics are reasonably precise and give evidence that the magnetometer measurements as a group were at the limit of resolution, with few, if any, bad readings.

Table 14
Orbit Statistics from Biased, Recalibrated PQV Statistics

Orbit	$\tilde{\sigma}_{Arc}$	$\tilde{\sigma}_{RA}$	$\tilde{\sigma}_{Dec}$
1063	0°.39	0°.02	0°.39
1068	0.50	0.04	0.50
1072	0.50	0.04	0.50
1083	0.59	0.03	0.59
1088	0.48	0.04	0.48
1093	0.29	0.03	0.29
1098	0.59	0.06	0.59
1103/1104	0.80	0.07	0.80
1108	0.45	0.04	0.45
1113	0.68	0.06	0.68
1118	0.48	0.03	0.48
1124	0.56	0.05	0.56
1128	0.77	0.05	0.77

Advantages and Disadvantages of the Four Approaches

The four approaches to cone intersection solutions of the spacecraft spin axis presented in this report are all in use on one or more of the satellite data reduction systems at Goddard Space Flight Center, and each has limitations or liabilities as well as the proven capability of producing satisfactory solutions.

The critical problem for the cone intersection methods for spacecraft without the time measured between sensor readings occurs as the two intersection points of two cones approach each other and the initial estimate is not necessarily closest to the true solution. For the IDCT and CFLS/PQ least-squares approaches, data separated in time as widely as

feasible provide multiple vectors, with sufficiently different cone angles, to select unambiguously the proper solution. The non-least squares approaches, producing multiple solutions for each complete telemetry time interval based on each ambiguity in the data, must be augmented by time histories showing interval-to-interval status of the solutions. In this way, however, slow changes in the spin axis due to external torques can be detected and followed.

In order for the least squares approaches to follow a slowly-moving spin axis, alterations in the algorithms have been designed which utilize the overdetermined nature of the equations to solve for the initial position, RA_0, Dec_0, or X_0, Y_0, Z_0; the rates of change, $\dot{RA}$, $\dot{Dec}$, or $\dot{X}$, $\dot{Y}$, $\dot{Z}$; and rates of change of the rates of change, $\ddot{RA}$, $\ddot{Dec}$, or $\ddot{X}$, $\ddot{Y}$, $\ddot{Z}$; such that, for some time Δt after the initial time t_0, the spin axis position components are given by

$$RA = RA_0 + \dot{RA} \cdot \Delta t + \ddot{RA} \cdot \Delta t^2$$

$$Dec = Dec_0 + \dot{Dec} \cdot \Delta t + \ddot{Dec} \cdot \Delta t^2$$

or

$$X = X_0 + \dot{X} \cdot \Delta t + \ddot{X} \cdot \Delta t^2$$

$$Y = Y_0 + \dot{Y} \cdot \Delta t + \ddot{Y} \cdot \Delta t^2$$

$$Z = Z_0 + \dot{Z} \cdot \Delta t + \ddot{Z} \cdot \Delta t^2 .$$

The greatest limitation on the least-squares approaches occurs during periods of rapid spin-axis reorientation maneuvers, when the overdetermined telemetry data is inconsistent with good attitude solutions.

The chief difference in the least-squares methods is in the computation complexity of the IDCT over the CFLS. By relying on a single pass through the algorithm steps, the CFLS method is faster than the more complex and iterated IDCT, although solutions may be slightly more accurate from the IDCT.

Goddard Space Flight Center
National Aeronautics and Space Administration
Greenbelt, Maryland July 1974
311-07-14-01-51

PAGES MISSING FROM AVAILABLE VERSION

REFERENCES

1. Goldstein, Herbert, *Classical Mechanics*, Reading, Mass., Addison-Wesley Publishing Co., Inc., 1950.

2. Thomson, W. T., *Introduction to Space Dynamics*, New York, John Wiley & Sons, Inc., 1961.

3. Fang, A. C., *An Approach to Attitude Determination for a Spin-stabilized Spacecraft (IMP I)*, NASA TN D-6925, August 1972.

4. Pyle, E. J., *IMP I Optical Aspect System*, NASA TN D-7008, March 1971.

SOURCES

Brown, T., M. Moulding, and R. Shaw, *Small Astronomy Satellite–A Preprocessor Program*, NAS 5-11790, Task 168, Silver Spring, Md., Computer Science Corporation, July 1971.

Computer Science Corporation, *Solar Aspect and Magnetometer Attitude Program Description*, Silver Spring, Md.

Fischell, R. E., and R. B. Kershner, *Attitude Control System for a Small Astronomy Satellite*, Silver Spring, Md., Johns Hopkins University Applied Physics Laboratory.

Johns Hopkins University Applied Physics Laboratory, *NASA SAS-A Satellite System Design and Interface Requirements*, Silver Spring, Md., May 1968.

Marion, J. B., *Classical Dynamics*, New York, Academic Press, Inc., 1965.

Schlegal, L. B., *Cones: An Iterative Differential Correction Technique for Attitude Determination of a Spinning Satellite*, NAS 5-10022, Gaithersburg, Md., IBM, May 1967.

APPENDIX A

EULER ANGLES

A spacecraft with body-fixed axes xyz and an inertial system with coordinates XYZ is considered. (See figure A-1.) To transform xyz into XYZ, a series of three rotations about initial and intermediate axes is the maximum number required, regardless of the relative orientation of the two sets of axes. These rotations are known as Euler angles. They are not unique. That is, the general solution of the transformation of any right-handed orthogonal coordinate system into another coordinate system can be characterized by several different sets of Euler angles. The first rotation can be about any axis—x, y, or z. If the first rotation axis selected is the z, then several angles of rotation leading to the desired transformation are possible. Specifically, these angles may be the rotations of y into either the ZY, zY, zX, ZX, or zZ planes. There are two intersections of the rotation of y about z with each of the above planes giving ten possible choices of the rotation. Similarly, there are 10 possible choices for the rotation of the x-axis about the z-axis into the five planes.

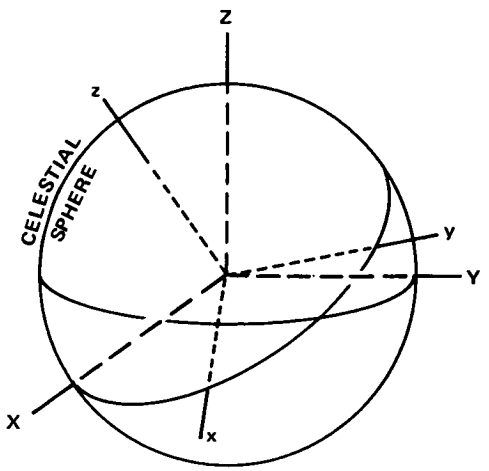

Figure A-1. Spacecraft xyz Axes and Inertial Coordinates XYZ

This first rotation is necessary in order to position the transformed axes with respect to the fixed axes, in such a way that the second rotation brings one transformed axis into coincidence with the desired fixed axis. The first rotations indicated above satisfy this condition for one of two reasons. Either the rotation of an axis into a plane formed by a fixed axis and the axis of rotation places the third transformed axis perpendicular to that plane from which the second rotation about the perpendicular axis is made; or the rotation of an axis into a plane formed by two fixed axes allows the second rotation to be about this axis, such that the appropriate axis is made both perpendicular to the fixed axis plane and coincident with the third fixed axis. The second rotation having transformed one axis into one fixed axis, the third rotation is about these coincident axes and completes the transformation.

Obviously, if the first axis of rotation had been the x or y rather than the z, parallel statements could be made. Thus, 30 first rotations are possible. The second and third rotations are dictated by the first, resulting in the 30 different transformations.

As illustrations of the above (see figure A-2), the following rotations are considered: The transformation of x-, y-, z-axes into X-, Y-, Z-axes by an initial rotation around the z-axis (by angle θ), moving the x-axis into the XY plane; second, a second rotation about the new x-axis until the z-axis coincides with the Z-axis (angle ϕ); and third, a final rotation around the z=Z axis (by an angle ψ).

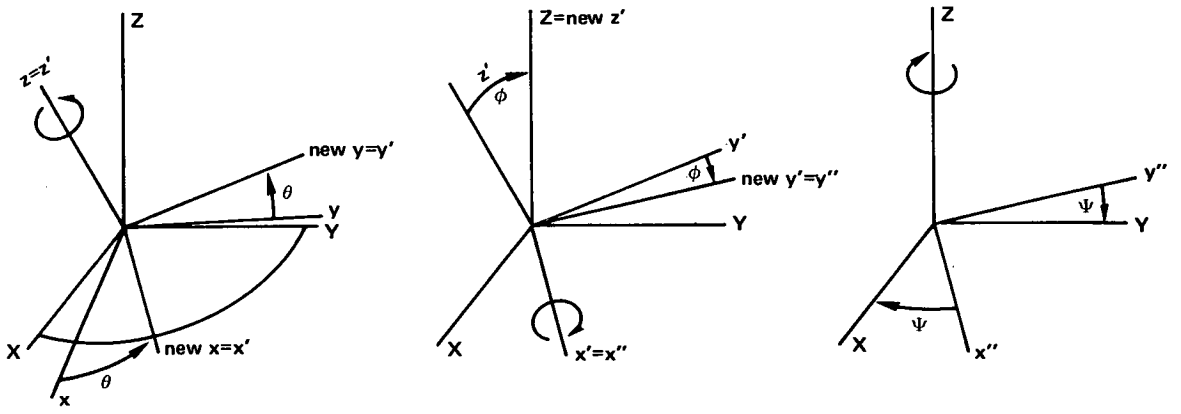

(a) Initial Rotation about z-axis

(b) Rotation about new x'-axis

(c) Final Rotation about Z-axis

Figure A-2. Rotation of Spacecraft Axes

Each rotation can be described mathematically by analytic geometry or by matrix theory. Thus,

$$z' = z; \qquad z'' = (-\sin\phi)\,y' + (\cos\theta)\,z'; \qquad z''' = z'' = Z$$

$$x' = (\cos\theta)\,x + (\sin\theta)\,y; \qquad x'' = x'; \qquad x''' = (\cos\psi)\,x'' + (\sin\psi)\,y'' = X$$

$$y' = (-\sin\theta)\,x + (\cos\theta)\,y; \qquad y'' = (\cos\phi)\,y' + (\sin\theta)\,z'; \qquad y''' = (-\sin\psi)\,x'' + (\cos\psi)\,y'' = Y$$

or more compactly,

$$\begin{bmatrix} x' \\ y' \\ z' \end{bmatrix} = \begin{bmatrix} \cos\theta & \sin\theta & 0 \\ -\sin\theta & \cos\theta & 0 \\ 0 & 0 & 1 \end{bmatrix} \begin{bmatrix} x \\ y \\ z \end{bmatrix}; \qquad \begin{bmatrix} x'' \\ y'' \\ z'' \end{bmatrix} = \begin{bmatrix} 1 & 0 & 0 \\ 0 & \cos\phi & \sin\phi \\ 0 & -\sin\phi & \cos\phi \end{bmatrix} \begin{bmatrix} x' \\ y' \\ z' \end{bmatrix};$$

$$\begin{bmatrix} X \\ Y \\ Z \end{bmatrix} = \begin{bmatrix} \cos\psi & \sin\psi & 0 \\ -\sin\psi & \cos\psi & 0 \\ 0 & 0 & 1 \end{bmatrix} \begin{bmatrix} x'' \\ y'' \\ z'' \end{bmatrix}$$

The total transformation is even more convenient by using matrix notation. Instead of algebraically substituting to get

$$Z = Z(x, y, z, \theta, \phi, \psi);\quad X = X(x, y, z, \theta, \phi, \psi);\quad Y = Y(x, y, z, \theta, \phi, \psi),$$

the matrix product–

$$\begin{bmatrix} X \\ Y \\ Z \end{bmatrix} = \begin{bmatrix} \cos\psi & \sin\psi & 0 \\ -\sin\psi & \cos\psi & 0 \\ 0 & 0 & 1 \end{bmatrix} \begin{bmatrix} 1 & 0 & 0 \\ 0 & \cos\phi & \sin\phi \\ 0 & -\sin\phi & \cos\phi \end{bmatrix} \begin{bmatrix} \cos\theta & \sin\theta & 0 \\ -\sin\theta & \cos\theta & 0 \\ 0 & 0 & 1 \end{bmatrix} \begin{bmatrix} x \\ y \\ z \end{bmatrix}$$

$$\begin{bmatrix} X \\ Y \\ Z \end{bmatrix} = \begin{bmatrix} \cos\psi\cos\theta - \sin\psi\cos\phi\sin\theta & \cos\psi\sin\theta + \sin\psi\cos\phi\cos\theta & \sin\psi\sin\phi \\ -\sin\psi\cos\theta - \cos\psi\cos\phi\sin\theta & -\sin\psi\sin\theta + \cos\psi\cos\phi\cos\theta & \cos\psi\sin\phi \\ \sin\phi\sin\theta & -\sin\phi\cos\theta & \cos\phi \end{bmatrix} \begin{bmatrix} x \\ y \\ z \end{bmatrix}$$

provides the desired relationships. These are the Euler rotations used in Goldstein (reference 1, p. 107), with constraints $0 \leqslant \psi < 2\pi$, $0 \leqslant \phi < \pi$, $0 \leqslant \theta < 2\pi$.

An important convention should be noted. Angles are considered positive for counter-clockwise rotations and negative for clockwise rotations. The rotations in illustration A-2 are ccw for θ, and cw for ϕ and ψ; therefore, the angles ϕ and ψ are negative.

Next, the following rotations are considered (figure A-3): The transformation of xyz into XYZ by an initial rotation around the x-axis (by an angle ξ), moving the z-axis into the xZ plane; a second rotation about the new y-axis (perpendicular to the xz'Z plane), until the z'-axis coincides with the Z (angle ζ); and a final rotation around the $z'' = Z$ axis (by an angle η), which brings x into X and y into Y.

$$\begin{bmatrix} X \\ Y \\ Z \end{bmatrix} = \begin{bmatrix} \cos\eta & \sin\eta & 0 \\ -\sin\eta & \cos\eta & 0 \\ 0 & 0 & 1 \end{bmatrix} \begin{bmatrix} \cos\zeta & 0 & -\sin\zeta \\ 0 & 1 & 0 \\ \sin\zeta & 0 & \cos\zeta \end{bmatrix} \begin{bmatrix} 1 & 0 & 0 \\ 0 & \cos\xi & \sin\xi \\ 0 & -\sin\xi & \cos\xi \end{bmatrix} \begin{bmatrix} x \\ y \\ z \end{bmatrix}$$

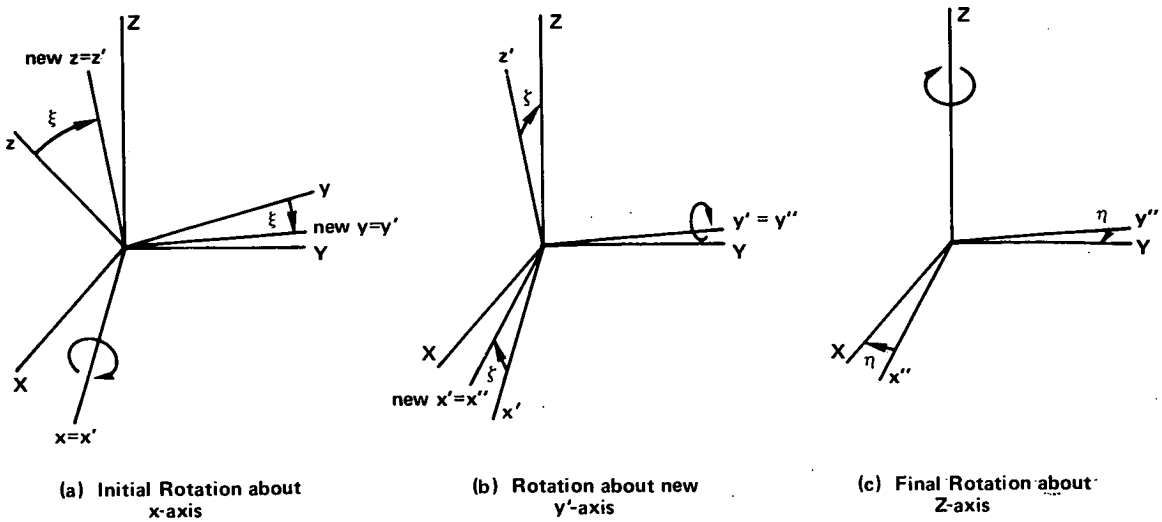

(a) Initial Rotation about x-axis

(b) Rotation about new y'-axis

(c) Final Rotation about Z-axis

Figure A-3. Rotation of Spacecraft Axes

APPENDIX B

SPACECRAFT SENSORS

SUN SENSORS

The sensor angle derived from the digital sun sensor is the angle between the spacecraft spin axis and the vector from the spacecraft to the sun. This vector is computed from ground information of the instantaneous positions of the spacecraft and the sun in geocentric inertial coordinates.

The most commonly used digital sun sensor has photocells arranged in 10 columns, produces nine bits, and indicates the sun angle to within 0°.5. To minimize the number of photocells, the array design places the cells in a pattern which requires various-sized cells overlapping many rows. One such pattern is shown in figure B-1.

The long dimension of the box-shaped sensor is mounted perpendicular to the spin axis and is centered in the xy-plane. There are two slits with 180° fields of view, such that every point on the celestial sphere is within the fields of view once each spin period. A long sun-angle slit, in the xy-plane, permits the sun's rays to fall on a particular row of cells across nine columns, and the array is constructed in such a way that the resulting 1- and 0-bits indicate a particular sun angle. If a photocell in a particular column is excited, the corresponding binary digit in a telemetry word is a 1-bit. If the light passes over a blank cell, the corresponding bit is a 0-bit. The bits are read out in order by the telemetry electronics, and eventually are decoded on the ground.

The second slit, the command slit, is parallel to the spin axis. The sun image from this slit falls only on the first column of photocells. When the sun image first falls on this column an electronic pulse initiates a counter, and the next sequential pulse stops the counter. The sensor electronics centers each pulse with respect to the total time that the sun is viewed by the particular photocells, and the resulting total count between two pulses provides data on the spacecraft spin period.

MAGNETOMETERS

Magnetometers, which define cone angles for use in attitude determination, measure the magnetic field components along three mutually orthogonal axes. The magnetic field components from such a triaxis magnetometer define the magnetic field vector in spacecraft coordinates for a particular universal time. The field vector in inertial coordinates is also known at that time from spacecraft orbit and magnetic field model computations. These two separate vector representations can be related to derive a unique cone angle between the inertial coordinate field vector and a possible spin axis orientation.

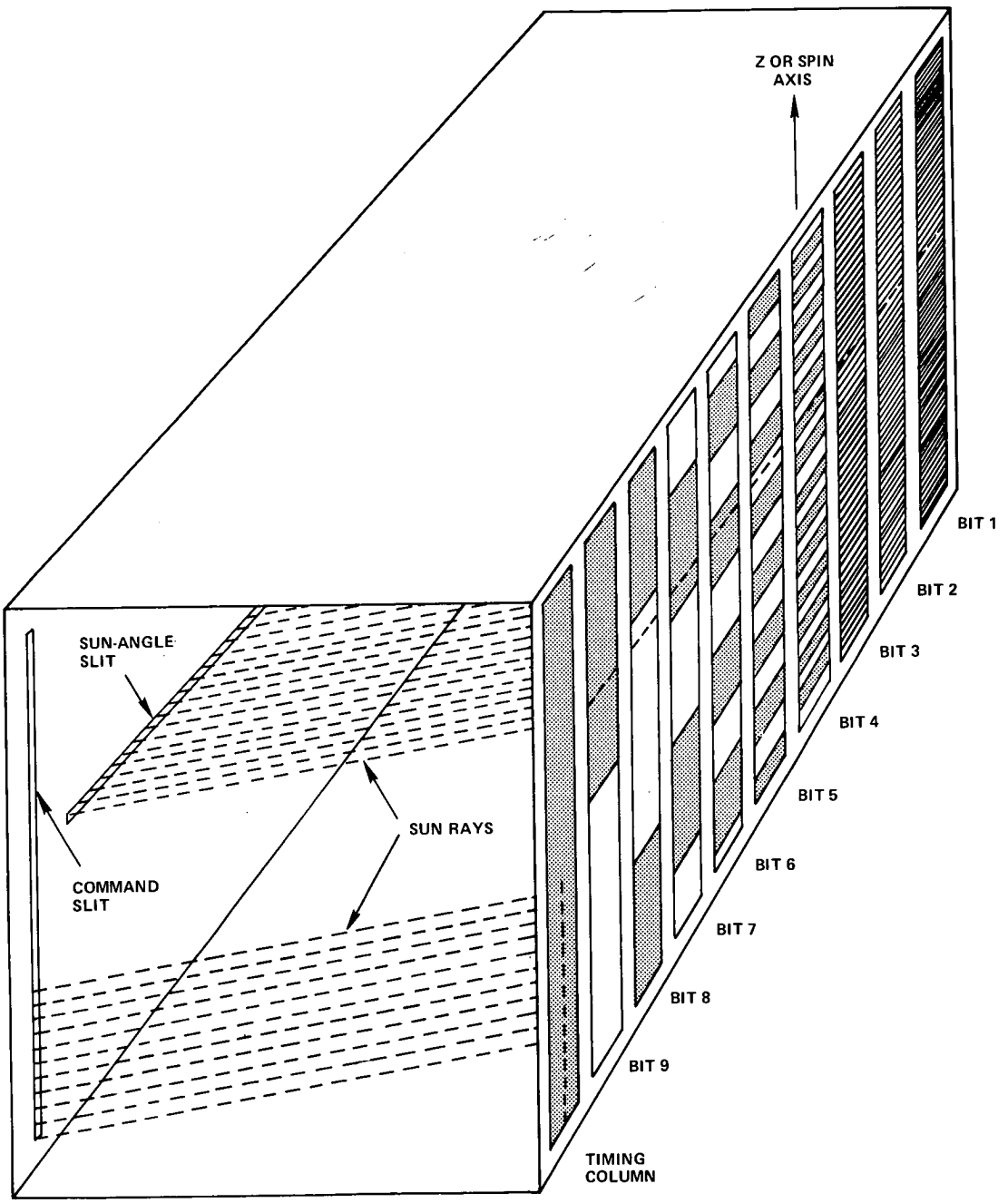

Figure B-1. Nine-bit Solar Sensor

One triaxis magnetometer consists of three Shönstedt induction magnetometers, each aligned along a spacecraft axis with a sensitivity of ±27.853 milliamperes/meter (±350 milli-oersteds). The three field components must be sampled sequentially by the spacecraft telemetry, but the magnetic field vector changes slowly with respect to the telemetry sampling, such that no appreciable error is introduced. The time of measurement of the components is determined by the known time lag from sampling the magnetometers to the samples entering the telemetry, by the known spacecraft relative time of the telemetry magnetometer sample words, and by the cycling speed of the spacecraft telemetry related to universal time (deduced on the ground after transmission of the data).

Spacecraft orbit positions for given universal times are computed from orbit elements produced from ground observations of the spacecraft. These orbit positions have associated magnetic field vectors which are closely approximated by complex field models. The models are especially accurate for spacecraft altitudes between 300 and 2000 km. The field model vectors are transformed to inertial coordinates, and serve as the known reference vectors for cone-angle evaluation.

The cone angles are constructed from the magnetic field components measured by the triaxis magnetometer. If the components in spacecraft coordinates are represented by M_x, M_y, and M_z, then the cone angle μ (figure B-2) is determined from

$$\cos \mu = \frac{M_z}{\sqrt{M_x^2 + M_y^2 + M_z^2}}$$

where, as before, the spacecraft z-axis is the spin axis. For a magnetic field vector $\vec{H}_i$ (in inertial coordinates), corresponding to the spacecraft external magnetic field at spacecraft position $\vec{P}_i$, the spin axis must have coordinates of a point on a circle of radius μ_i about the vector $\vec{H}_i$ (figure B-3).

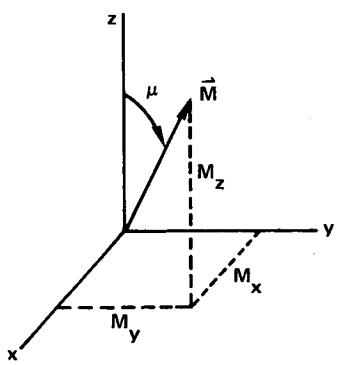

Figure B-2. Magnetic Field Vector

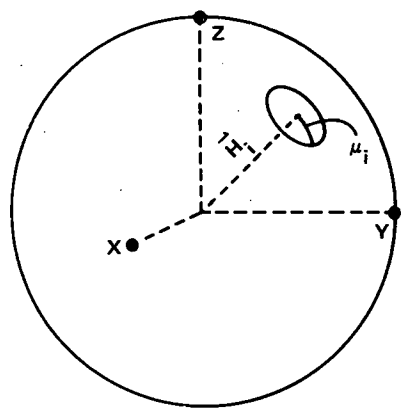

Figure B-3. Magnetic Field Vector in Inertial Coordinates with Cone of Possible Axis Positions

EARTH HORIZON SENSORS

One class of earth sensors used in cone-intersection attitude-determination systems consists of a telescope with a narrow field of view, mounted at a known angle γ ($\approx 90°$) to the spacecraft spin axis. It contains a sensing element to detect the change in visible light intensity between the sunlit earth and space or between the sunlit earth and the shadowed earth, and also the associated electronics to control the counters required for attitude solutions. Additional data, however, are required before the earth-horizon-sensor readouts lead to the cone angle of interest, the angle between the spin axis and the earth nadir. These data include (1) the earth center vector, (2) sun sensor data, (3) relations between the sun and the earth, (4) orbit information, and (5) reduction algorithms. The sun relations and the algorithms to find the desired relations are necessary because the earth is not a point source, as the sun can be considered to be, and the earth sensor readings are in relation to points on the horizon, not to the earth center.

The earth center vector is easily derived from orbit determination, since the position vector, $\vec{P}$, of the spacecraft referenced from the earth center is opposite in sign to the earth center vector, $\vec{E}$, referenced from the spacecraft. Thus, the components

$$P_X = -E_X, P_Y = -E_Y, P_Z = -E_Z .$$

By this the earth center coordinates are known. Then, if the earth sensor, at a known angle γ to the spin axis, produced a pulse only on sighting the center of the earth, the cone-intersection parameters would be known. Unfortunately, the earth sensor provides two pulses triggered by two unknown points on the earth horizon (figure B-4) or one unknown point on the earth horizon and one unknown point on the earth terminator, where the terminator is the division between the sunlit earth and the shadowed earth. Also, by means of the counters measures are made of the earth chord between the two unknown horizon/terminator points, of the sun-to-earth horizon time (earth time), of the telemetry-to-spacecraft sensor time (sun time), and of the successive sun sightings (the spin period). The earth chord is often inaccurately called "earth width" in the literature and that convention will be followed here.

The telemetry readouts of the counter provide the means of relating the center-of-earth vector to the unknown horizon vectors. The counters are driven by a constant oscillator of C_n counts/second. Thus the spin period, SP, is determined in seconds from the number of counts in the spin period counter, C_{sp}, and the count rate, C_n, by

$$SP = C_{sp}/C_n .$$

Similarly, the earth time is $E_t = C_{E_t}/C_n$, the earth width is $EW = C_{E_W}/C_n$, and the sun time is $S_t = C_{S_t}/C_n$, all in seconds of time. The earth time is expressed as the angle between the sun/spin axis plane and the earth horizon/spin axis plane through the relation

$$\nu \text{ (in degrees)} = \frac{E_t}{SP} \times 360° .$$

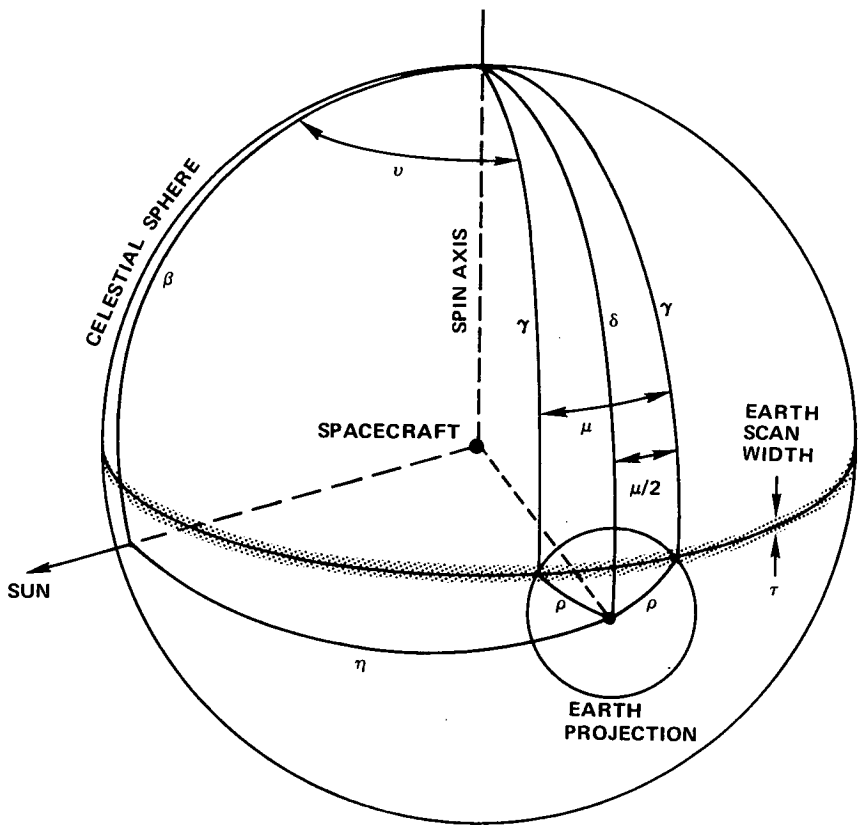

Figure B-4. Earth Horizon Sensor Relations

Similarly, the earth width is written as an angle relation by

$$\mu \text{ (in degrees)} = \frac{E_W}{\overline{SP} \times 360^\circ} .$$

The sun sensor produces the sun angle β between the spin axis and the sun. Orbit information supplies the angle η between the sun and the earth center (negative spacecraft position vector). The angular radius of the earth ρ is derived from

$$\sin \rho = \frac{Re}{R}$$

where R_e = the radius of the earth, and

R = the spacecraft position magnitude.

NOTE: ρ is half the *true* angular earth width.

With these parameters, the earth nadir angle δ, between the spin axis and the earth center, can be determined as required for a second cone angle. Two earth-sun-spacecraft relations can exist, which allow and affect algorithms necessary to find δ. If from the spacecraft the earth is completely shadowed, no solution of δ is possible; if the earth is completely sunlit, a comparatively simple algorithm making use of the half angle of μ is used. If an earth terminator is visible, additional auxiliary angles between the earth horizon and the sun are formed, since the earth terminator is not directly useful. The two relations–for two horizons and one horizon/one terminator–are developed in two different algorithms in the section, "Some Non-least Squares Methods of Solution."

One other problem in dealing with earth-horizon sensors concerns the angular diameter of the telescope field of view. This angular diameter or scanning angle τ causes the sensor photodiode pulse to trigger the earth horizon counters when a certain percent of the field of view is filled by the sunlit earth. In general, the pulse is not exactly coincident with the center of the field of view crossing the earth horizon. Therefore, the resultant counts are proportionately larger or smaller than an exact count. This generates a systematic error, which with some difficulty is largely eliminated.

APPENDIX C

RESOLUTION OF SPIN-AXIS AMBIGUITY

If a spacecraft has two sensors—a $\vec{P}$ vector sensor and a $\vec{Q}$ vector sensor—to provide measurements for the determination of the spacecraft spin axis $\hat{S}$, the vector relations of the section, "The Unique Solution, Three-constraint (PQV) Approach," are applicable, that is,

$$\hat{P} \cdot \hat{S} = \cos\beta, \qquad \hat{Q} \cdot \hat{S} = \cos\delta, \qquad \hat{P} \times \hat{Q} = \vec{V} = \sin\eta\,\hat{V},$$

$$\hat{Q} \times \hat{P} = -\vec{V}, \qquad \hat{P} \cdot \hat{Q} = \cos\eta$$

where $\hat{S}$ has a two-solution ambiguity. In addition to these vector relations, the spin period (SP) of the spacecraft, the time ($T'_{P\rightarrow Q}$) between sensor sightings, and the angle (ϵ) between the two sensors in the spin (xy) plane must be known or measured. Let $\hat{S}_1$ and $\hat{S}_2$ be the two separate spin axis solution vectors, with

$$\hat{V} \cdot \hat{S}_1 = -\hat{V} \cdot \hat{S}_2 = \cos\alpha\,.$$

The convention is to define the spacecraft spin axis as the axis, viewed from above the spacecraft, about which the spacecraft spins ccw. The adjusted time is

$$T_{P\rightarrow Q} = T'_{P\rightarrow Q} + \frac{\epsilon}{360^\circ} \times SP$$

where $\epsilon/360^\circ \times SP$ is positive whenever the $\vec{P}$ vector sensor lags behind the $\vec{Q}$ vector sensor as the spacecraft spins. Typically, an attempt is made to align the sensors in the spacecraft xz plane to eliminate or minimize this factor.

The selection of the correct spin axis solution is made by the following test:

$$\text{If } \alpha < 90^\circ \text{ and } T_{P\rightarrow Q} < \tfrac{1}{2}\,SP$$

or

$$\text{if } \alpha > 90^\circ \text{ and } T_{P\rightarrow Q} > \tfrac{1}{2}\,SP,$$

then $\hat{S} = \hat{S}_1$; otherwise, $\hat{S} = \hat{S}_2$. Refer to figure C-1 for geometrical relations.

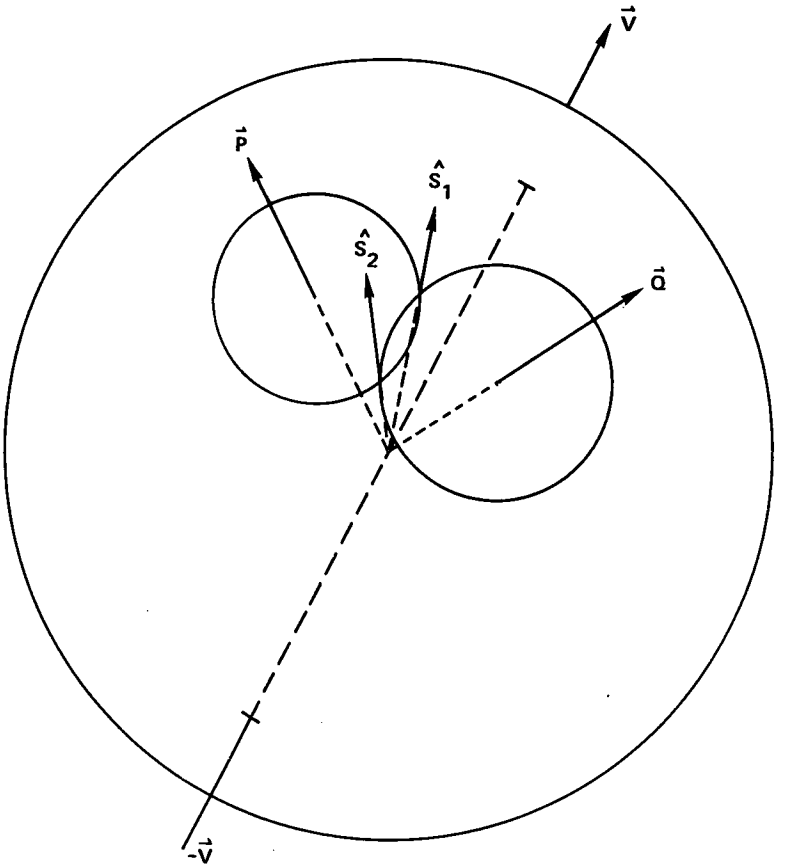

Figure C-1. The Two-solution Spin-axis Ambiguity

APPENDIX D

THE METHOD OF LEAST SQUARES

A set of n linear equations,

$$\underset{\text{measured}}{Y_i} \approx \underset{\text{calculated}}{aX_i + b} \qquad (i = 1, 2, \ldots, n),$$

is overdetermined if $n > 2$, in that just two relations of measured Y_i at a given X_i are needed to solve unambiguously for a and b, but errors in the measured values Y_i will not result in the same coefficients a and b for every choice of (X_i, Y_i) (figure D-1). The requirement of a single set of the slope and Y intersection coefficients a and b, which makes the defined line closest in some sense to all of the measurements, is a problem often encountered.

A least-squares best fit of the data is one widely used method to determine the coefficients, not only in the simple linear case, but also in many other applications. The linear case will motivate the discussion, but the results in matrix notation are general and can be applied wherever the matrix forms can be defined with a linear set of coefficients.

The method called least squares refers to the mathematical procedure followed in which the differences or residuals (figure D-2) between the measured and calculated values,

$$Y_i - (aX_i + b) = r_i \qquad \text{(condition equations)},$$

are squared and summed over all points, the sum of the squares

$$\sum_{i=1}^{n} r_i^2$$

is minimized with respect to the coefficients a and b, and the resulting two equations are solved for a and b. Since the sum of the squares is a function of a and b,

$$\sum_{i=1}^{n} r_i^2 = f(a, b),$$

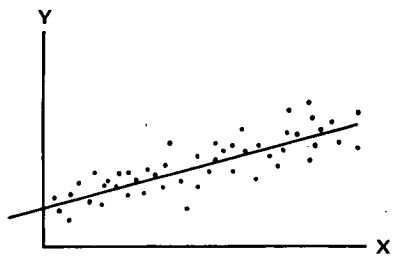

Figure D-1. Measured versus Calculated Values

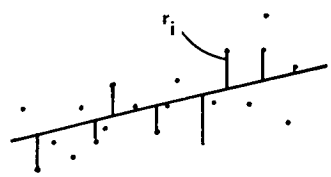

Figure D-2. Residuals between Measured and Calculated Values

minimizing the function is done by taking the partial derivatives with respect to a and with respect to b and setting them to zero:

$$\frac{\partial f(a, b)}{\partial a} = 0, \qquad \frac{\partial f(a, b)}{\partial b} = 0.$$

The particular a and b for which these conditions hold simultaneously define the function f (a, b) such that f is a minimum (that is, f has a greater value for any other choice of a and b).

Carrying out the partial differentiations and solving for a and b,

$$\frac{\partial f(a, b)}{\partial a} = 2 \sum_{i=1}^{n} (Y_i - b - aX_i)(-X_i) = 0 = 2 \sum_{i=1}^{n} (aX_i^2 + bX_i - X_iY_i)$$

$$\frac{\partial f(a, b)}{\partial b} = 2 \sum_{i=1}^{n} (Y_i - b - aX_i)(-1) = 0 = 2 \sum_{i=1}^{n} (aX_i + b - Y_i)$$

or

$$\left.\begin{aligned} a \sum_{i=1}^{n} X_i^2 + b \sum_{i=1}^{n} X_i &= \sum_{i=1}^{n} X_iY_i \\ a \sum_{i=1}^{n} X_i + nb &= \sum_{i=1}^{n} Y_i \end{aligned}\right\} \quad \text{(normal equations)}$$

wherefore

$$a = \frac{n \sum_{i=1}^{n} Y_iX_i - \sum_{i=1}^{n} Y_i \sum_{i=1}^{n} X_i}{n \sum_{i=1}^{n} X_i^2 - \left(\sum_{i=1}^{n} X_i \right)^2}$$

$$b = \frac{\sum_{i=1}^{n} X_i^2 \sum_{i=1}^{n} Y_i - \sum_{i=1}^{n} X_iY_i \sum_{i=1}^{n} X_i}{n \sum_{i=1}^{n} X_i^2 - \left(\sum_{i=1}^{n} X_i \right)^2}$$

The same results are produced by an equivalent but more convenient matrix least-squares approach. The initial set of linear equations is given by

$$\begin{bmatrix} Y_1 \\ Y_2 \\ \cdot \\ \cdot \\ \cdot \\ Y_n \end{bmatrix} = \begin{bmatrix} X_1 & 1 \\ X_2 & 1 \\ \cdot & \cdot \\ \cdot & \cdot \\ \cdot & \cdot \\ X_n & 1 \end{bmatrix} \begin{bmatrix} a \\ b \end{bmatrix}$$

where the approximations and residuals do not enter explicitly into the matrix approach.* In representational form,

$$\underset{(n \times 1)}{Y} = \underset{(n \times 2)}{X} \; \underset{(2 \times 1)}{C} \qquad \text{(condition equations).}$$

Premultiply by the transpose of X to square the prematrix of C

$$\underbrace{\underset{(2 \times n)}{X^T} \; \underset{(n \times 1)}{Y}}_{(2 \times 1)} = \underbrace{\underset{(2 \times n)}{X^T} \; \underset{(n \times 2)}{X} \; \underset{(2 \times 1)}{C}}_{(2 \times 1)} \qquad \text{(normal equations).}$$

If the (2 X 2) X^TX matrix is nonsingular, it has an inverse and

$$\underset{(2 \times 2)}{(X^TX)^{-1}} \; \underset{(2 \times 1)}{X^TY} = \underset{(2 \times 1)}{C}$$

which in expanded form is

$$\begin{bmatrix} \dfrac{n}{n\sum_{i=1}^{n} X_i^2 - \left(\sum_{i=1}^{n} X_i\right)^2} & \dfrac{-\sum_{i=1}^{n} X_i}{n\sum_{i=1}^{n} X_i^2 - \left(\sum_{i=1}^{n} X_i\right)^2} \\ \dfrac{-\sum_{i=1}^{n} X_i}{n\sum_{i=1}^{n} X_i^2 - \left(\sum_{i=1}^{n} X_i\right)^2} & \dfrac{\sum_{i=1}^{n} X_i}{n\sum_{i=1}^{n} X_i^2 - \left(\sum_{i=1}^{n} X_i\right)^2} \end{bmatrix} \begin{bmatrix} \sum_{i=1}^{n} X_iY_i \\ \sum_{i=1}^{n} Y_i \end{bmatrix} = \begin{bmatrix} a \\ b \end{bmatrix}$$

*Smith, G. A., *The Theory and Application of Least Squares*, GSFC TMX 63127, December 1967.

This is the result obtained by squaring residuals, summing, minimizing, and solving for a and b.

Certain equations involving nonlinear parameters can be solved for these parameters by the least-squares method using an iterative process. Beginning with a set of nonlinear equations and an initial estimate of the desired parameters, the equations are linearized and solved for corrections to the initial estimate. The corrections are added to make a new estimate and the procedure is repeated if the corrections are not less than preselected limits.

Since the required parameters–coefficients such as a and b or components of other relations–are not involved in a simple, linear fashion in the defining equations, these defining equations are linearized by expanding in a Taylor's series about the required parameters, truncating the series after the linear terms, and evaluating the function at the estimated solution. Assume a general function, $f_i = f_i\,(Y_i, X_i, A_k) = 0$ ($i = 1, 2, \ldots, n$; $k = 1, 2, \ldots, m$), is composed of a set of n equations which are nonlinear in the m coefficients A_k. Expanding in a Taylor's series about A_k evaluated at the estimate A_k°,

$$f_i\,(Y_i, X_i, A_k) = f_i\,(Y_i, X_i, A_k^\circ) + \sum_{k=1}^{m} \left(\frac{\partial f_i}{\partial A_k}\right)_{A_k = A_k^\circ} \Delta A_k + O\,(\Delta A_k)^2 + \ldots$$

where

$$\Delta A_k = (A_k - A_k^\circ).$$

For additional notational simplicity, let

$$f_i\,(Y_i, X_i, A_k^\circ) = f_i^\circ \quad \text{and} \quad \left(\frac{\partial f_i}{\partial A_k}\right)_{A_k = A_k^\circ} = \frac{\partial f_i}{\partial A_k^\circ}.$$

Then the expansion truncated after the ΔA_k terms is

$$f_i\,(Y_i, X_i, A_k) \approx f_i^\circ + \sum_{k=1}^{m} \frac{\partial f_i}{\partial A_k^\circ} \Delta A_k \approx 0.$$

Switching to matrix notation to complete the solution of the corrections ΔA_k,

$$-\begin{bmatrix} f_1^\circ \\ f_2^\circ \\ \cdot \\ \cdot \\ \cdot \\ f_n^\circ \end{bmatrix} = \begin{bmatrix} \partial f_1/\partial A_1^\circ & \partial f_1/\partial A_2^\circ & \cdot & \cdot & \cdot & \partial f_1/\partial A_m^\circ \\ \partial f_2/\partial A_1^\circ & \partial f_2/\partial A_2^\circ & \cdot & \cdot & \cdot & \partial f_2/\partial A_m^\circ \\ \cdot & \cdot & \cdot & & & \cdot \\ \cdot & \cdot & & \cdot & & \cdot \\ \cdot & \cdot & & & \cdot & \cdot \\ \partial f_n/\partial A_1^\circ & \partial f_n/\partial A_2^\circ & \cdot & \cdot & \cdot & \partial f_n/\partial A_m^\circ \end{bmatrix} \begin{bmatrix} \Delta A_1 \\ \Delta A_2 \\ \cdot \\ \cdot \\ \cdot \\ \Delta A_m \end{bmatrix}$$

$(n \times 1)$ $(n \times m)$ $(m \times 1)$

or

$$-F = P\Delta$$

where F = the matrix of function equations evaluated with the estimated coefficient A_k°,

P = the matrix of partial differentiations, and

Δ = the matrix of coefficient correction elements.

The procedure for solving for Δ is identical to the first case of solving for C since the equations are now linear in Δ, such that

$$\Delta = -(P^T P)^{-1} P^T F .$$

The correction elements are compared with the preselected limits E_k and depending on the comparison results, different actions are taken. If some $\Delta A_k > E_k$, then new estimates

$$A_k^\circ = A_k^\circ + \Delta A_k$$

are formed and the process is repeated. If all $A_k \leqslant E_k$, then the final, acceptable solutions are formed

$$A_k = A_k^\circ + \Delta A_k .$$

NATIONAL AERONAUTICS AND SPACE ADMINISTRATION
WASHINGTON, D.C. 20546

OFFICIAL BUSINESS
PENALTY FOR PRIVATE USE $300

SPECIAL FOURTH-CLASS RATE
BOOK

POSTAGE AND FEES PAID
NATIONAL AERONAUTICS AND
SPACE ADMINISTRATION
451

U.S.MAIL

POSTMASTER: If Undeliverable (Section 158 Postal Manual) Do Not Return

"The aeronautical and space activities of the United States shall be conducted so as to contribute . . . to the expansion of human knowledge of phenomena in the atmosphere and space. The Administration shall provide for the widest practicable and appropriate dissemination of information concerning its activities and the results thereof."

—NATIONAL AERONAUTICS AND SPACE ACT OF 1958

NASA SCIENTIFIC AND TECHNICAL PUBLICATIONS

TECHNICAL REPORTS: Scientific and technical information considered important, complete, and a lasting contribution to existing knowledge.

TECHNICAL NOTES: Information less broad in scope but nevertheless of importance as a contribution to existing knowledge.

TECHNICAL MEMORANDUMS: Information receiving limited distribution because of preliminary data, security classification, or other reasons. Also includes conference proceedings with either limited or unlimited distribution.

CONTRACTOR REPORTS: Scientific and technical information generated under a NASA contract or grant and considered an important contribution to existing knowledge.

TECHNICAL TRANSLATIONS: Information published in a foreign language considered to merit NASA distribution in English.

SPECIAL PUBLICATIONS: Information derived from or of value to NASA activities. Publications include final reports of major projects, monographs, data compilations, handbooks, sourcebooks, and special bibliographies.

TECHNOLOGY UTILIZATION PUBLICATIONS: Information on technology used by NASA that may be of particular interest in commercial and other non-aerospace applications. Publications include Tech Briefs, Technology Utilization Reports and Technology Surveys.

Details on the availability of these publications may be obtained from:

SCIENTIFIC AND TECHNICAL INFORMATION OFFICE

NATIONAL AERONAUTICS AND SPACE ADMINISTRATION

Washington, D.C. 20546